METHODOLOGY FOR PREDICTING MICROELECTRONIC SUBSTRATE WARPAGE INCORPORATING COPPER TRACE PATTERN CHARACTERISTICS

A Dissertation

Presented to

The Academic Faculty

by

Luke McCaslin

In Partial Fulfillment

of the Requirements for the Degree

Master of Science in Mechanical Engineering

Georgia Institute of Technology

August 2008

METHODOLOGY FOR PREDICTING MICROELECTRONIC SUBSTRATE WARPAGE

INCORPORATING COPPER TRACE PATTERN CHARACTERISTICS

Approved by:

Dr. Suresh Sitaraman, Chairman
School of Mechanical Engineering
Georgia Institute of Technology

Dr. Russell Peak
Manufacturing Research Center
Georgia Institute of Technology

Dr. Charles Ume
School of Mechanical Engineering
Georgia Institute of Technology

Date Approved: June 5, 2008

ACKNOWLEDGEMENTS

I would like to thank my advisor, Dr. Sitaraman, for his support and encouragement in this process. I am also grateful to Dr. Russell Peak and Dr. Charles Ume for agreeing to serve on my thesis committee and for other valuable comments. I would also like to thank Samson Yoon at Samsung Techwin for his helpful comments during the course of my work.

My sincere thanks goes out to my fellow members of the CASPaR lab. Without the support, knowledge and friendship of Jamie, Krishna, Karan, Kevin, Injoong, Xi, Nick, and Greg my time here would have been greatly extended and far less enjoyable. I also appreciate the support which my family and my wife, Austin have given in this process. I would also like to thank God for the opportunity to study at Georgia Tech, and for the strength to complete the task.

TABLE OF CONTENTS

LIST OF TABLES

LIST OF FIGURES

LIST OF ABBREVIATIONS

BGA – Ball Grid Array

CSP – Chip Scale Package

CTE – Coefficient of Thermal Expansion

DIP – Dual In-line Package

DOF – Degrees of Freedom

FEM – Finite Element Method

I/O – Input/ Output

IC – Integrated Circuit

IR – Infrared

MEMS – Micro-electro-mechanical systems

MIPS –Million Instructions per Second

PGA – Pin Grid Array

PWA – Printed Wiring Board Assembly

PWB – Printed Wiring Board

QFP – Quad Flat Package

SBU – Sequential Build Up

SMT – Surface Mount Technology

TMA – Thermomechanical Analyzer

LIST OF SYMBOLS

11, 22, 12, 21 = Longitudinal, transverse, major, and minor directions

a – Distance from the neutral plane to the bottom of the copper traces

b – Copper trace thickness

°C – Degrees Celsius

E – Young's Modulus

f – Fiber property

G = Shear modulus

GPa – Gigipascals

I – Bending moment of inertia

K – Degrees Kelvin

m – Matrix property

M – Moment of inertia

MPa – Megapascals

Ppm – Parts per million

U - Displacement

V = Volume fraction

Vf – Volume fraction of copper

w – Trace pitch

x – X coordinate direction

y – Y coordinate direction

z – Z coordinate direction

α = CTE

θ – θ direction in Hough transform space

ρ – ρ direction in Hough transform space

υ = Poisson's ratio

SUMMARY

The current trend in electronics manufacturing is to decrease the size of electronic components while attempting to increase processing power and performance. This is leading to increased interest in thinner printed wiring boards and finer line widths and wire pitches. However, mismatches in the thermomechanical properties of materials used can lead to warpage, hindering these goals. Warpage can be problematic as it leads to misalignments during package assembly, reduced tolerances, and a variety of operational failures.

Current warpage prediction techniques utilize isotropic volume averaging to estimate effective material properties in layers of copper mixed with interlayer dielectric material. However, these estimates do not provide material properties with sufficient accuracy to predict warpage, as they contain no information about the orientation of the copper traces. This thesis describes the development of a new technique to predict the warpage of a particular substrate. The technique accounts for both the trace pattern planar density and planar orientation in determining effective orthotropic material properties for each layer of a multi-layer substrate. Starting with the trace pattern image, this technique first divides the trace pattern into several smaller areas for a given layer of the substrate and then uses image processing techniques to determine the copper percentage and average trace orientation in each small area. The copper percentage and average trace direction orientation are used in conjunction with the material properties of copper and the dielectric material to calculate the effective orthotropic material properties of each smaller area of the substrate.

A finite-element model is then created where each layer is represented as a concatenation of several small areas with independent directional properties, and such a model is then subjected to sequential thermal excursion as seen in the actual fabrication process. The results from the models have been compared against experimental data with a great degree of accuracy. The modeling technique and the results obtained clearly demonstrate the need for the proposed subdivisional orthotropic material property calculations, as opposed to homogeneous isotropic properties typically used for each layer in computational simulations, as these more accurate directional properties are capable of predicting warpage with higher accuracy.

CHAPTER 1

INTRODUCTION

Warpage, or the out of plane displacement of an electronic package due to mismatches in thermomechanical properties of the constituents of the package, is a growing problem in the microelectronics industry. Warpage leads to an array of problems for microelectronics manufacturers, such as lead shortening, solder fatigue, and alignment difficulties. To fully understand and investigate the issue of thermomechanically induced warpage in microelectronics packages, knowledge of the microelectronics industry, specifically microelectronics manufacturing and electronic package manufacturing, is required.

Microelectronics manufacturing is a set of complex chemical and physical processes used to make the active components in a large variety of electronic products. Electronic packaging, which is a step in the overall microelectronics manufacturing procedure, is the set of processes which are incorporated to ensure the electrical components in a system are interconnected electrically and protected mechanically. The process steps which effect warpage will be discussed in detail later. Modeling of the warpage induced by these processes is the focus of this research.

1.1 Microelectronics Manufacturing

The microelectronics industry has its roots in the mid-1900s, with the invention of the transistor in 1947 and the first integrated circuit (IC) in 1959. Since then, the industry

has grown at a remarkable pace, staying on track with Moore's Law, which predicted that the number of connections on a silicon chip would double every 18-24 months. Microelectronics has expanded to include optoelectronics, micro-electro-mechanical systems (MEMS), and nanotechnology. With incredibly diverse end products such as computers, cellular phones, digital cameras, and telecommunications equipment, the microelectronics industry is estimated to be in the multi-trillion dollar range. Most microelectronic systems are based around silicon chips, which perform the tasks of processing and memory for the system.

The microelectronics manufacturing process begins with making silicon chips. The first step starts with a single-crystal silicon boule. The highly purified silicon is then sliced into thin wafers. Wafers are cleaned and polished to obtain a pure, flat, and regular surface in preparation for the next steps. Areas of the silicon wafer are altered chemically to define regions of devices on the chip and isolate devices from each other. Photolithography processing is utilized to define features. Ions of doping materials are deposited onto the wafers to beneficially alter electrical characteristics of features in defined areas. Metallization of the wafer provides interconnects between devices on the wafer as well as a means to provide external connection to the processed chips. These processes are repeated until the chips are fully formed on the wafer. After this, the wafer is diced into individual chips and each chip is tested. After the chips have been produced, they are housed in electronic packages.

Electronic packages form the link from the chip to the rest of the electronic device, providing electrical interconnections to route signals from the chip to the rest of the device as well as the connections which provide power to the chip. They also protect the

chip against mechanical loads and shocks as well as harmful radiation. Packages also assist in the removal of the excessive heat produced by the chip. Electronic packages themselves require a complicated set of steps in their manufacture. The steps relevant to this work are concerned with manufacturing the package substrate which provides the connection from the silicon chip to the rest of the device.

Packaging substrates and printed wiring boards (PWBs) are typically made by the process known as sequential build up (SBU) or some variation of it. The SBU process begins with an insulating core material, such as FR4, which has been clad with copper. A photo-resist layer is applied to the copper and then photo exposed in the desired trace pattern to cure. The unnecessary copper is etched away and the photo-resist is removed. A dielectric layer is then applied and cured using infrared (IR) or convection heating or some combination of the two. This dielectric layer provides insulation between successive layers of metallization. Vias, which provide interconnection between layers of copper can then be added by another masking and curing process. Another layer of photo-resist is then applied and cured in the desired pattern for the next copper layer. This process is repeated until the substrate has the desired number of layers. A schematic of this process is shown in Figure 1.1. The processing steps involving curing of dielectric layers lead to the warpage of the substrate.

Note that this process places dielectric material between copper traces. This complicates the calculation of the effective material properties for these layers, as it is difficult to estimate the properties of the composite dielectric and copper matrix.

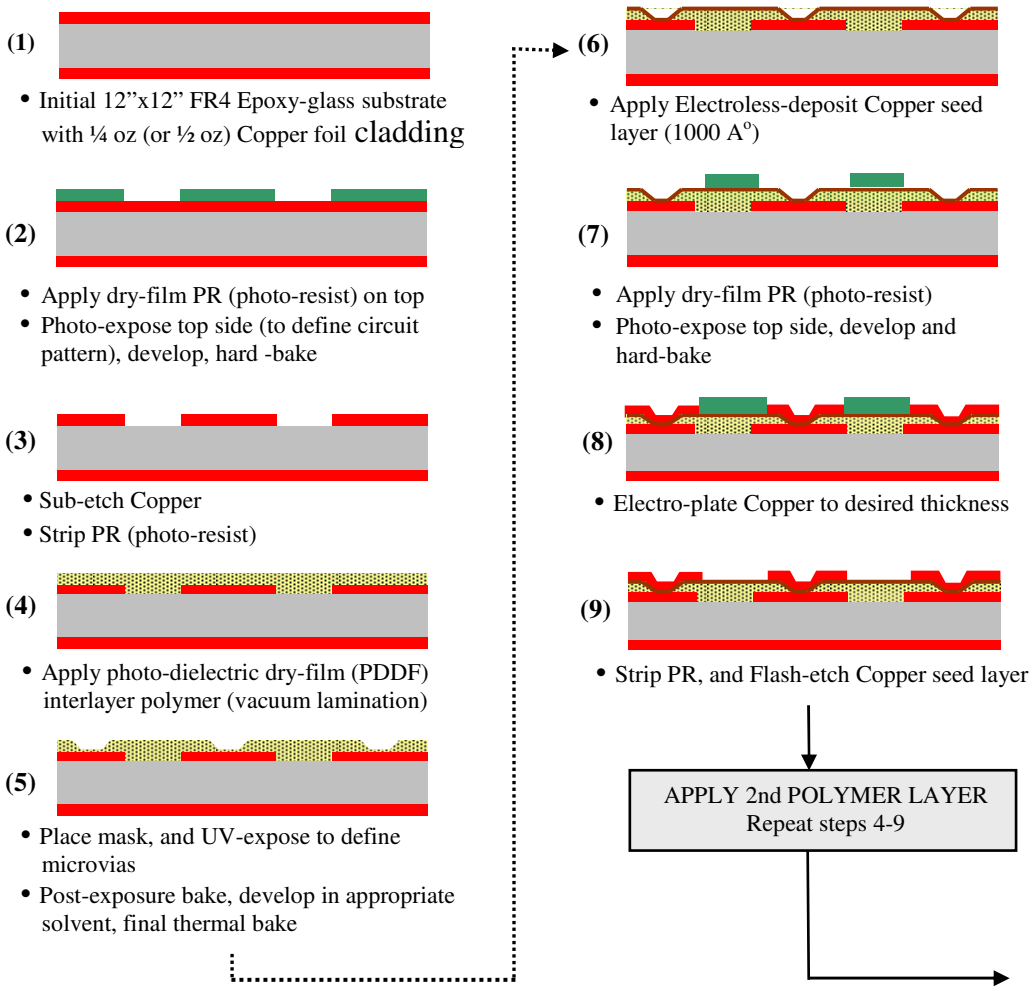

Figure 1.1: Schematic of SBU process steps [Dunne 2000]

1.2 Microelectronics Packaging and Trends

Electronic packaging was defined by Tummala and Rymaszewski [1989] as “the science and art of establishing interconnections and a suitable operating environment for predominantly electrical circuits to process or store information.” Electronic packages perform the functions of heat dissipation, signal interconnection, mechanical protection, and providing power to the chip.

Performance of electronic packages is essential to overall IC performance. Figure 1.2 shows the factors affecting circuit performance in Million Instructions per Second (MIPS). Delays due to chip logic have been reduced drastically, but the performance of packages has fallen behind this progress, causing packages to become a barrier to increased electrical performance [Lau and Erasmus 1993].

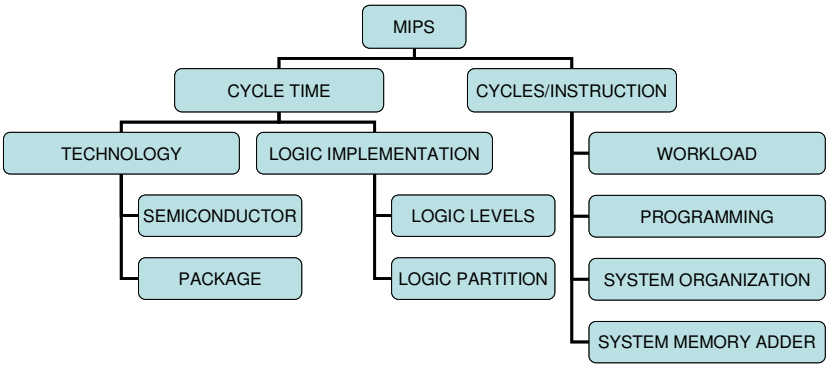

$$Performance\ (MIPS) = \frac{1000}{cycle\ time\ X\ cycles\ per\ instruction}$$

Figure 1.2: Factors effecting package performance [Tummala and Rymaszewski 1989]

Packaging technologies have changed over the years to keep pace with rapidly increasing demand for faster signal speed, higher input/ output (I/O) count, lower cost, and better thermal performance. This has caused the development of a large number of packaging technologies.

In the 1970's electronic packages were largely in the form of the Dual In-line Package (DIP), which have pin I/Os along the side of the package. Pin Grid Array (PGA) packages were developed to achieve a higher I/O count by having the I/Os arranged in an area array. Small outline packages were developed for lower I/O count requirements, such as in memory applications. Quad Flat Packages (QFPs) were developed as an extension of small outline packages to have a higher I/O count. Space limitations have

caused the development of surface mount technology (SMT) such as Ball Grid Array (BGA) packages which have a much smaller footprint on a printed wiring board (PWB) because of their area array distribution of interconnects. These packages are smaller and have a higher I/O count than their predecessors, and deliver superior electrical performance due to the shortened lead distance of a solder ball. Chip Scale Packages (CSPs), where the package is nearly the same size as the chip, were developed in the 1990's for increased performance and decreased size. Figure 1.3 shows the development of electronic packages over the past 30 years.

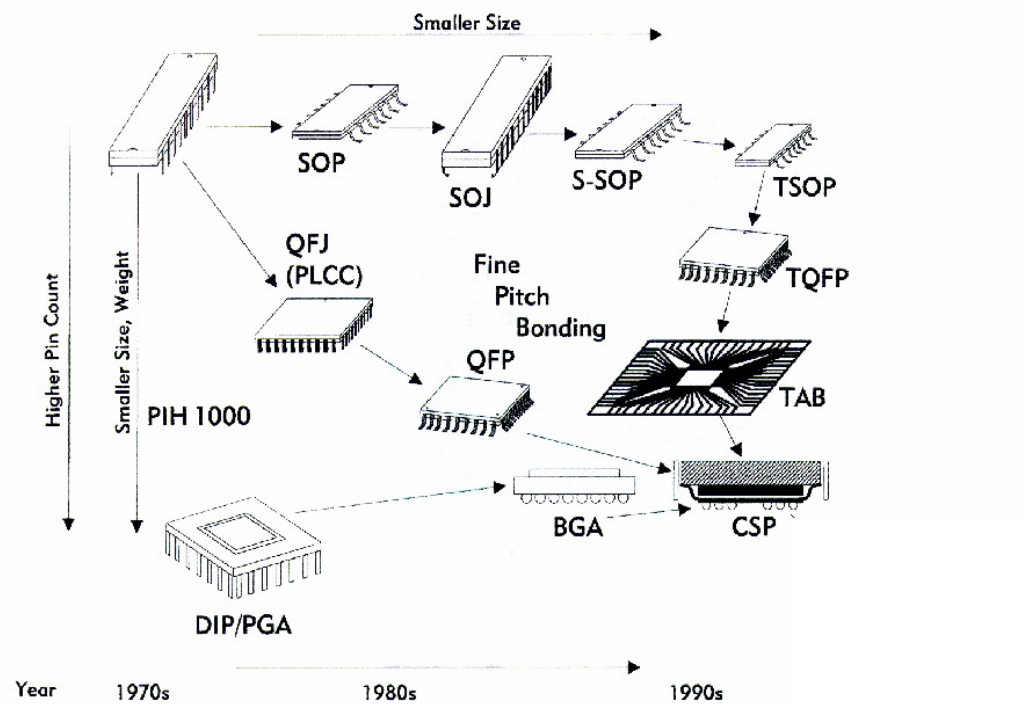

Figure 1.3: Evolution of single chip packages [Rymaszewski et al., 1999]

The overall trend of electronic packages has been toward smaller size, increased electrical and thermal performance, and increased I/O count and density, as shown in Figure 1.3. This tendency is causing an overall decrease in trace widths and wire pitches, leading to a decrease in alignment tolerances. This decrease in tolerances has made

warpage an important issue. For instance, for line widths of 100 microns, warpage of 50 microns results in a 30% error in the photo-resist pattern transferred by the masking process [Banerji et. al. 2002].

1.3 Warpage

Warpage can come from a variety of sources. Mechanical loading, shrinkage from the cure of interlayer dielectric material, moisture, and temperature variation are the chief causes of warpage. Temperature variation is looked at as the primary source, and is the subject of most technical studies of warpage. An electronic package is made from a variety of materials, such as layers of copper traces which are used to conduct signals and power and the interlayer dielectric materials. These materials alternate and often compose four or more layers.

Since each material has a different coefficient of thermal expansion (CTE), each material wants to expand to a different length when heated. Each layer of dielectric material must be cured, often at temperatures of 150°C or higher. When the dielectric layer is cured, it is in a stress free state at its cure temperature. When the substrate is cooled after the cure step both the dielectric and copper try to contract at different rates. This is the driver for thermomechanically induced warpage.

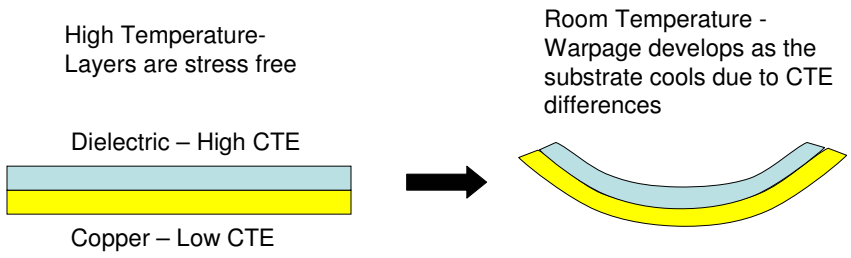

Figure 1.4: Warpage development

The prediction of the warpage of an electronic package substrate is difficult and many approximations are required to perform this task. Specifically, approximations are often made to reduce the complexity of the material systems involved in packaging. For instance, core materials such as FR-4 consist of an interwoven glass cloth which has been impregnated with an epoxy material and then cured. Such materials are usually described as homogeneous and orthotropic, an approximation which works well for warpage predictions.

Copper traces are often geometrically complicated, and a multilayered substrate will have multiple layers of complicated patterns. The modeling of such networks is considered to be too difficult for analytical techniques and is typically carried out using the finite element method (FEM). However, the exact modeling of such complex shapes is difficult even for FEM and requires too many elements and too much processing time. Therefore most strategies of predicting substrate warpage involve using some method of effectively representing copper properties so that they can be modeled more easily.

A popular approach to the reduction in complexity of the copper trace pattern is the volume average approach, in which the properties of copper traces are calculated by a linear average of properties of the copper and dielectric materials. This approach yields isotropic material properties for mixed material layers. Therefore, with this approach two trace patterns such as those shown in Figure 1.5 would be determined to have the same material properties.

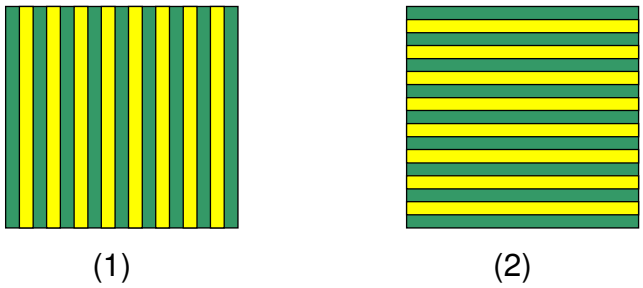

Figure 1.5: Copper trace patterns with identical material by the volume average approach

Since the modulus of elasticity of copper is about an order of magnitude higher than that of the typical dielectric material, the pictured sections should be much stiffer in one direction than the other. This shows that the simple volume average approach may not be sufficient to calculate the material properties of mixed copper and dielectric layers. With this in mind, this research undertakes the task of finding a method to account for the direction of the copper traces when calculating the material properties of mixed copper and dielectric layers.

1.4 Warpage Due to Alternate Processing Approaches

The SBU process for manufacturing substrates and PWBs was highlighted earlier. In this process the substrate is typically flat during the dielectric cure step. However, in one variation of the SBU process, where the processing occurs in a reel to reel fashion, as shown in Figure 1.5, the substrate will be on a reel and therefore bent when the cure step occurs. If the dielectric cure step is performed while the substrate is held mechanically in a bent position, the dielectric will be stress free when at the elevated temperature and held in this bent position. It is reasonable to assume that this process will have an effect on warpage.

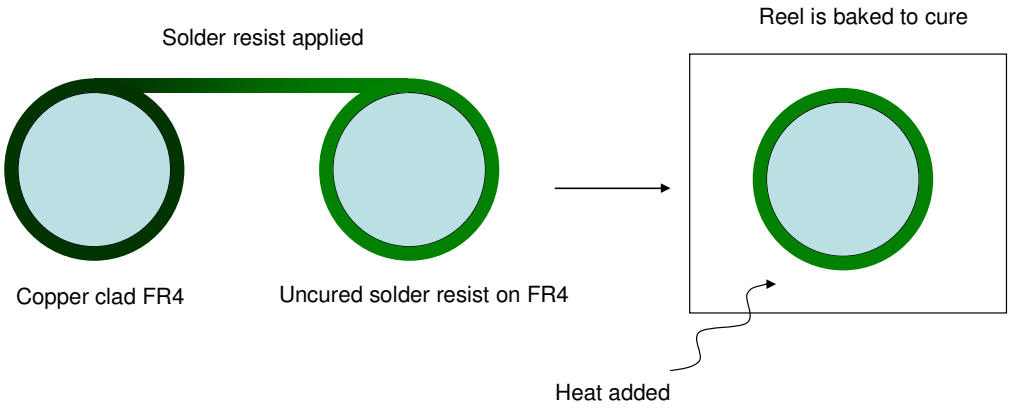

Figure 1.6: Demonstration of solder resist application in the reel to reel process

CHAPTER 2

LITERATURE REVIEW

Rigorous study of warpage in PWBs and substrates has been undertaken by many researchers. A brief review of these studies gives understanding of the current approaches to warpage prediction and gives insight into the direction future research should take. This review will also discuss causes of warpage and give strategies which have previously been used to capture each effect in the modeling process. As PWBs and substrates in electronic packages are made by similar processes, contain the same materials, and serve a similar function, the causes of warpage in each will be considered to be the same.

2.1 Problems Caused by Warpage

The difficulties associated with excessive warpage have been well documented. Warpage causes difficulty in aligning masks for definition of traces and vias. In fact, the percentage of via displacement with respect to its intended position, normalized by the via diameter, was 25% for warped substrates [Banerji et. al. 2002]. Warpage causes an increase in stresses which can lead to cracking of the silicon die [Ranjan et. al. 1998]. Stresses from warpage can also contribute to the delamination of layers in the substrate [Wang et. al. 2000]. Warpage is also a driver for solder fatigue, which can result in solder cracking and product failure [Lee 1998].

These problems have made warpage responsible for a large financial cost to the microelectronics industry. Therefore, warpage prediction and reduction strategies have been a much researched topic.

2.2 Causes of Warpage

There are three main causes of warpage in PWBs and package substrates. These are shrinkage of the polymer dielectric layer during the cure process, swelling of layers due to hygroscopic stresses induced by moisture absorption, and thermal stresses caused by mismatches in the CTE of materials in different layers of the substrate. The contribution to warpage from each of these mechanisms must be examined to fully understand warpage.

Chemical shrinkage occurs during the dielectric cure step. In this step, the polymer chains which make up the dielectric material crosslink when heated to form a stiff matrix. When the polymer chains crosslink they take up less volume, causing the material to shrink. This process has been quantified by several researchers. Changes in sample dimensions at various stages in the cure process have been measured directly [White and Hahn 1992]. There are also many other more sophisticated techniques, such as those involving dilatometry, density measurements, or use of a thermomechanical analyzer (TMA). However, since the cure process involves heating the dielectric to high temperatures, often above its glass transition temperature, T_g, it is believed that stresses due to chemical shrinkage are relieved by viscous deformation of the dielectric [Harper 1983]. This means that warpage is mostly caused by the combined forces of hygroscopic stresses and thermal stresses.

Warpage due to hygroscopic stresses arises when different materials absorb different quantities of moisture. This causes the composite body to swell unevenly, causing warpage. This phenomenon has been studied by several researchers [Douglass et. al., 1980; Farley et. al. 1978]. The effects of such swelling are difficult to predict.

However, if a substrate is baked prior to warpage measurement, moisture contained in the substrate can be evaporated, leaving thermal stresses as the only warpage driver left to consider.

The primary cause of warpage is considered by many researchers to be thermal stresses due to mismatches in the CTE of different layers. Researchers have studied the effects of thermomechanical mismatches on silicon wafers [Lee & Tobin, 1986], effects of thermomechanical mismatches in various stages of PWB processing [Polsky, 2000; Ume 1997], process induced warpage of substrates for multi-chip modules [Dang et. al. 2000], and for BGA packages [Verma et. al. 1999].

2.3 Warpage prediction strategies

As warpage is a large problem for the microelectronics industry, many methods have been developed to predict warpage. These approaches have focused on many different aspects of warpage. A large amount of information about warpage prediction strategies comes from analysis of laminates. Since this information is relevant to the study of warpage, a brief analysis of it will be presented here.

Lamination theory has been used to estimate the behavior of thin composites for some time. Lamination theory is based on the assumption that layers in a composite behave like thin plates. Further assumptions about the stress state of the composite structure reduce the problem from three dimensions to two dimensions [Reddy et. al. 1989]. Daniel et. al. (1990) used lamination theory to predict the warpage and stresses in a multilayered composite structure and the results were shown to compare well with shadow moiré measurements. Wang et. al. (1992) developed an analytical model including viscoelasticity and cure shrinkage effects. This model was validated with

projection moiré and also aligned well with experimental data. Lamination theory was also used by Zewi et. al. (1986) to predict the residual stresses from differential thermal expansion of layers in a composite stack and predictions were validated by use of embedded strain gages and projection moiré. Interfacial stresses due to thermal mismatch have also been calculated using a variant of lamination theory [Xie and Sitaraman, 2000].

While lamination theory has been shown useful for several configurations of composite layered structures, the extremely complicated nature of material systems and trace pattern geometries in substrates yields itself quite well to analysis by finite element methods. A multitude of researchers have used FEM to predict process induced warpage of substrates and PWBs. A short summary of relevant work is shown here.

A study by Yeh et. al. (1991) used FEM to model the warpage of a PWB and validated predictions with use of a shadow moiré system. Accurate predictions were difficult to obtain, as true material properties were not used, but they were extracted from a number of publications. This study showed the importance of accurate material properties in the prediction of warpage. A sensitivity analysis was also conducted by Yeh et. al. (1993) which determined that the material properties with the strongest contribution to warpage were the CTE, Young's moduli, and layer thicknesses of the materials.

Analysis of the sensitivity of board warpage to solder masking material selection has also been conducted [Ume and Martin, 1997]. The study examined four asymmetric layouts using triangular shell elements. The study found that the CTE of the solder mask material was the most important in changing the warpage, followed by Young's Modulus, Poisson's ratio, and mask thickness.

The way in which heat is applied to substrates can also have a large effect on warpage. Polsky (2000) compared processes in which heat for solder reflow was applied evenly to the substrate, as in IR reflow, and processes in which a large thermal gradient is applied to the substrate, as in wave soldering. The study found that substrates which had IR heating applied had a much lower warpage than those which had the wave soldering process applied, due to the thermal gradient induced.

Studies have also been performed to find more accurate methods of modeling PWB warpage. Researchers have compared warpage predictions from 2D and 3D models [Yao and Qu, 1999]. Also, 2D and 3D models have been compared to a "2 ½ D" strip model which is a compromise between the two [Variyam and Sitaraman, 2000]. The study found that the 2 ½ D model is a good compromise between 2D and 3D models.

Researchers have also attempted to make models of printed wiring board assembly (PWA) structures, with all components in place on the PWB. The typical approach to modeling such a large structure is to parameterize and modularize the structure so that variations can be easily tested [Ding, 2003]. In this approach, individual components are constructed as modules independent of the other components and then combined to create the total model.

A methodology of reducing data from ECAD files which describe the trace pattern locations and other information about a PWB into a format which can be analyzed by FE models has been developed [Zwemer et al., 2004]. This methodology involves calculating the coefficient of thermal bending for various areas of a PWB to find areas which are large contributors to warpage. With this information, steps can be taken to reduce the warpage of the PWB.

Even with FEM, the geometric properties of constituents of a PWB can require too many elements and too much processing time to model conveniently. For this reason, researchers have tended to reduce the complexity of complicated composite materials by modeling them as a single orthotropic material. This is nearly always done with epoxy filled, woven laminates such as FR4. This approach is also often used to estimate the properties of substrate or PWB layers of mixed copper and dielectric material. Polsky (1998) applied a micromechanics approach to define orthotropic properties for copper trace patterns filled with dielectric based on the percentage of copper and the direction of the traces. However, the patterns used did not have the complication of a realistic trace pattern, as the pattern only involved straight lines. For this approach to be able to be applied to a real trace pattern, some method of detecting the effective direction of the traces in a particular layer must be developed.

Another strategy for calculating the effective areas is to use micromechanics equations to calculate orthotropic properties for a set of copper traces based on the volume percentage alone, and then assume that the traces are oriented randomly and calculate the effective properties as an average of the properties in the longitudinal and transverse directions [Ding, 2003]. However, trace patterns are often oriented in coherent directions in small areas, so this method may not be sufficient for predicting the effective properties in such areas.

A methodology known as the effective beam method has also been used to predict effective copper and dielectric properties. In this methodology, the copper traces are treated as a having a fraction of their actual thickness and the bending moment of inertia can be calculated by Equations 1.1, and 1.2.

$$I_{trace} = \int_{a}^{a+b} wV_f y^2 dy = \frac{wV_f a^3}{3}\left[3\frac{b}{a} + 3\left(\frac{b}{a}\right)^2 + \left(\frac{b}{a}\right)^3\right] \quad (1.1)$$

$$I_{unif} = \int_{a}^{a+bV_f} wy^2 dy = \frac{wV_f a^3}{3}\left[3\frac{b}{a} + 3V_f\left(\frac{b}{a}\right)^2 + V_f{}^2\left(\frac{b}{a}\right)^3\right] \quad (1.2)$$

Where the terms used are given in Figure 1.1 and can be described as:

I = bending moment of inertia

w = trace pitch

a = distance from the neutral plane to the bottom of the copper traces

b = copper trace thickness

V_f = volume fraction of copper

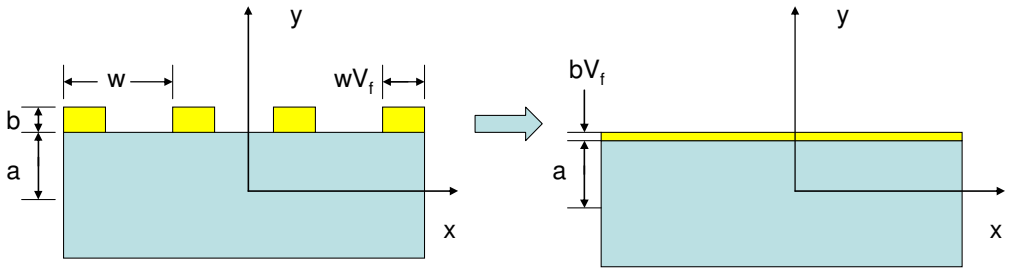

Figure 2.1: Parameters used for effective beam model [Ding 2003]

This approach has been shown to give similar results to the micromechanics approach [Ding, 2003]. However, neither of these approaches accounts for the orientation of the copper traces, and therefore may be inaccurate in some cases.

Grenestedt and Hutapea (2003) also developed a warpage prediction strategy based on using Kirchoff plate theory combined with Voight and Reuss formulations and

3D FE models to predict the properties of mixed copper and dielectric layers. This modeling effort attempted to tune the warpage of a PWB by moving copper between layers on the board to gain a balanced structure. The models showed that the warpage of a PWB could be greatly reduced by small changes in the copper trace pattern. Hutapea and Grenestedt (2004) also showed that the warpage in a PWB can also be reduced between 40 and 60 percent by giving the traces a wavy pattern. However, the altered electrical characteristics of such traces were a concern.

Some studies have used micro – macro models to reduce the number of elements required to model complicated structures. In this modeling methodology loads are applied to a global FE model of the structure. Then the local loads for a small section are applied to an exact model of that section to find the stresses and strains on elements in that small section. In 1993 Corbin applied this methodology to find the local stresses and strains in solder balls during thermal cycling. However, this methodology would be difficult to apply to warpage calculations, as global effects are the primary concern.

Other researchers have developed other schemes to reduce the complexity of models. One such methodology is nested finite element modeling, in which smaller elements are nested inside main elements in areas of stress or strain concentrations [Dharba and Dasgupta, 2001]. Another approach is to reduce the order of the stiffness matrices so the model is more computationally efficient [Reitz, 2002].

Steps can be taken to reduce warpage. An often suggested technique is attempting to match the CTE of all of the constituent materials to eliminate the property mismatches which cause interlayer stresses [Zweben, 2002]. However, given the number of materials required in the typical microelectronics application, it is nearly impossible to completely

avoid any thermomechanical mismatch. Another approach is to attempt to balance the copper percentage on each side of the substrate core in the hope that the stresses induced by the thermomechanical mismatches on either side of the board will balance out. However, this approach has been shown not to eliminate warpage, as the orientation of the copper traces is difficult to replicate on each side of the board, and failure to have the same pattern on each side of the board will lead to warpage [Hutapea and Grenestedt, 2007].

These approaches all work toward the goal of providing accurate models of warpage systems. For these modeling strategies to be applied with confidence they must be validated experimentally.

2.3 Experimental Validation Approaches

Even with the advances in modeling methodologies, the prediction of warpage based on models alone is not acceptable. Complicated structures such as package substrates require experimental validation to be carried out to show that the model predictions are accurate. There are several available techniques for experimental validation. Older techniques use contacting mechanical methods. The inaccuracies introduced by contacting the substrate during measurement have caused the development of non-contact techniques to measure warpage.

Most techniques used to measure warpage currently are optical methods. However, mechanical and electrical methods exist. Mechanical methods used to measure warpage typically consist of moving a gauge block relative to the surface to be measured and reading the warpage off of a gauge indicator. Electrical methods involve testing the

capacitance between the surface in question and a sensor. The distance change will show up as a change in capacitance [Ding, 2004]. These methods are not typically employed because they only provide point by point data, so it is difficult to construct a warpage profile for the entire surface.

Optical techniques are typically used to measure warpage. Shadow moiré and projection moiré are the most commonly used techniques, as they are non-contact, relatively inexpensive, and provide full field warpage data. Shadow moiré involves shining a light at an angle through a glass grating onto the warped surface. An overhead camera records the image of the grating and the shadow of the grating on the warped surface. These images are sent to a computer which uses them to calculate the warpage of the substrate. Projection moiré is similar to shadow moiré, except that instead of using a glass grating the grating is the projected image of an interference pattern of laser light [Ding, 2004]. Both systems are useful for measuring warpage, as they provide full field measurements and can be used to measure warpage at peak dielectric cure or solder reflow temperatures. Shadow moiré was used for validation purposes in this work.

CHAPTER 3

OBJECTIVES AND APPROACH

As previously stated, warpage is a large problem for the microelectronics industry. Current techniques used to predict warpage which use volume-averaged isotropic properties may not be sufficient to predict the warpage in the flexible substrates of the future. There is currently no published methodology which takes into account the direction of traces when calculating material properties for areas of mixed copper and dielectric. With this in mind, this thesis undertakes to accomplish the following goals:

1. Assess the viability of the volume average approach for predicting the effective properties of mixed copper and dielectric layers for application to FE models.
2. Develop a new modeling methodology which accounts for the direction of copper traces in the calculation of effective material properties of mixed copper and dielectric layers.
3. Build models of existing substrates with the developed modeling methodology
4. Validate developed approaches with experimental data from shadow moiré measurements.
5. Model the effects of the reel to reel process on substrate warpage.

To accomplish these goals, the following approaches will be followed:

1. Models of substrates with simple trace patterns will be constructed both by using the isotropic volume average approach and by modeling the trace

patterns exactly. The warpage predictions made by each of these models will be compared.

2. A methodology utilizing a Hough transform to detect lines in digital images of trace patterns will be developed to account for the directional characteristics of the trace pattern. Digital image processing techniques will also be employed to find the copper percentage in a given area of the substrate
3. Models of substrates with simple trace patterns will be constructed both by the developed methodology and by modeling the trace patterns exactly. The warpage predictions from each of these models will be compared.
4. Models will be made of production substrates using the described methodology and the warpage predictions from these models will be compared to experimental data obtained from shadow moiré experiments.

CHAPTER 4

EVALUATION OF THE ISOTROPIC VOLUME AVERAGING TECHNIQUE

Modeling the copper trace pattern of a packaging substrate is a difficult task. Trace patterns are typically far too complicated to be modeled with analytical methods, so FEM is often used. However, these patterns are often to complex for FEM to model exactly, so steps are taken to reduce the number of elements and computation time necessary to model trace patterns with FEM. An often used approach is to use micromechanics considerations to find effective material properties for layers of mixed copper and dielectric material. This approach yields isotropic properties for trace pattern layers based on the percentages of copper and dielectric present [Ding, 2003]. The effectiveness of this approach will be evaluated here. This methodology will be tested by using it to predict the warpage of a substrate with a simplified trace pattern and comparing this prediction to results of exact models made of the same substrate.

This approach calculates effective properties for mixed copper and dielectric layers with the assumption of complete randomness. However, this assumption is often invalid, as copper trace patterns generally run in a coherent direction in small areas of the trace pattern. This indicates that this approach may have difficulty in determining the effective properties of copper trace patterns which run in a well defined direction.

Effective material constants can be calculated for this approach by the following equations [Mallick, 1988; Herakovich, 1998]:

$$E_{11} = E_f V_f + E_m V_m \tag{3.1}$$

$$E_{22} = \frac{E_f E_m}{E_f V_m + E_m V_f} \tag{3.2}$$

$$\nu_{12} = \nu_f V_f + \nu_m V_m \tag{3.3}$$

$$\nu_{21} = \frac{E_{22}}{E_{11}} \nu_{12} \tag{3.4}$$

$$\alpha_{11} = \frac{\alpha_f E_f V_f + \alpha_m E_m V_m}{E_f V_f + E_m V_m} \tag{3.5}$$

$$\alpha_{22} = (1+\nu_f)\alpha_f V_f + (1+\nu_m)\alpha_m V_m - \alpha_{11}\nu_{12} \tag{3.6}$$

$$G_{12} = \frac{G_f G_m}{G_f V_m + G_m V_f} \tag{3.7}$$

Where E = Young's modulus

υ = Poisson's ratio

α = CTE

G = Shear modulus

V = Volume fraction

f, m = Fiber and matrix directions (respectively)

11, 22, 12, 21 = Longitudinal, transverse, major, and minor directions

If the copper trace orientation is assumed to be completely random, the effective modulus in any direction can be taken to be an average of E_{11} and E_{22}, and similar equations can be used for the CTE and Poisson's ratio:

$$E = \frac{E_{11} + E_{22}}{2} \tag{3.8}$$

$$\alpha = \frac{\alpha_{11} + \alpha_{22}}{2} \tag{3.9}$$

$$\upsilon = \frac{\upsilon_{12} + \upsilon_{21}}{2} \tag{3.10}$$

To test this methodology, an exact representation was made of a substrate with a trace pattern that could be modeled easily. This substrate is shown in Figure 3.1 and the stack-up of the materials used is shown in Figure 3.2. As seen in Figure 3.1, the substrate has a very simple trace pattern and quarter symmetry.

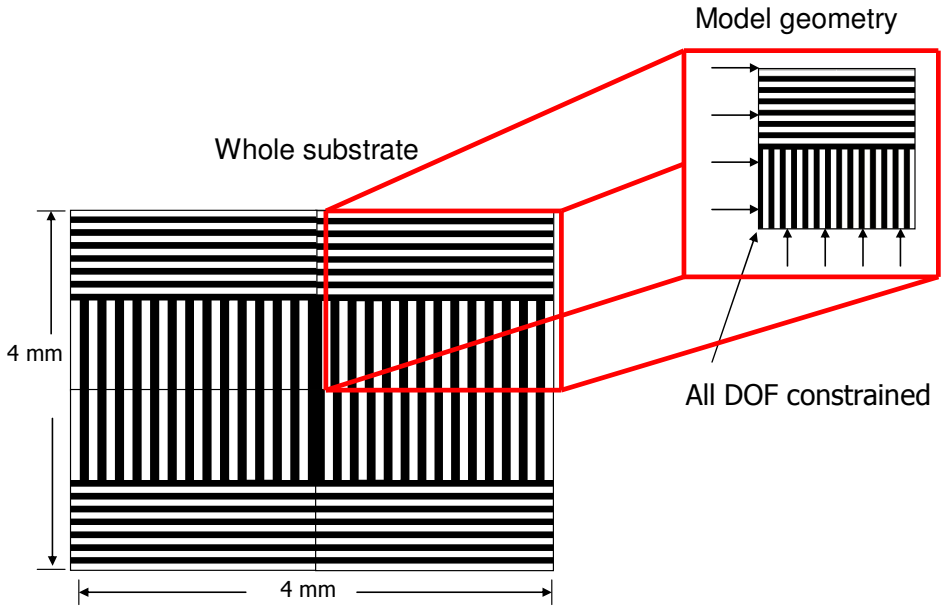

Figure 4.1: First substrate modeled to test previous methodology

Layer	Dimension (mm)
Solder resist top	0.04
FR-4	0.15
Copper	0.018
Solder resist bottom	0.03

Figure 4.2: Material stack-up for modeled substrate

The exact model was made using shell181 elements. To simulate cooling the substrate from a typical dielectric cure temperature to room temperature, the substrate was assumed to be stress free at 150°C and then it was cooled to 25°C. The material properties of the materials in the substrate are given in Tables 1.1-1.3. The symmetry in the substrate was taken advantage of by using quarter symmetric boundary conditions and constraining one node at the bottom left of the model in all degrees of freedom to prevent rigid body motion.

Table 4.1: FR4 Properties (Courtesy of Samsung Techwin)

MECHANICAL		THERMAL	
Young's Modulus	-	Density (kg/m^3)	193
Shear Modulus: G_{xz} (MPa)	693	Specific heat, c_p (J/kgK)	840
Shear Modulus: G_{xz} , G_{yz} (MPa)	199	Thermal Conductivity, κ (W/mK)	0.157
Poisson ratio: ν_{xz}	0.02		
Poisson ratio: ν_{xy}, ν_{yz}	0.1425		
CTE: α'_x,(ppm/K)	11.82		
CTE: α'_z (ppm/K)	13.34		
CTE: α'_y (ppm/K)	60.4 ($T<T_g$) 290 ($T>T_g$)		

Temp (°C) / Modulus	0	50	100	150
E_x (GPa)	19.01	16.97	15.17	13.22
E_z (GPa)	15.65	13.73	11.95	9.83
E_y (GPa)	1.625	1.600	1.575	1.550

Table 4.2: Copper properties (Polsky, 1998)

MECHANICAL		THERMAL	
Young's Modulus (GPa)	103.42	Density (kg/m^3)	8940
Poisson ratio	0.34	Specific heat, c_p (J/kgK)	384
Ultimate tensile strength, σ_{ult} (MPa)	275.8	Thermal Conductivity, κ (W/mK)	398
Yield stress, σ_y (MPa)	172.38		
CTE (ppm/K)	17.0		
Elongation at break (%)	12.0		

Table 4.3: Solder resist properties (Provided by Wong and Moon, Georgia Tech MSE Dept)

MECHANICAL							
Temperature (°C)		25	80	100	110	120	175
Young's Modulus (Mpa)		2412	1585	577	230	112	44
Poisson's Ratio	0.3						
CTE (ppm/K)	60						

A model was also made of the substrate using effective isotropic properties from the micromechanics approach. This model used the same boundary conditions and material stack-up as the exact model. The only difference was that instead of modeling

the trace pattern exactly, this model used equations 3.8-3.10 to calculate effective properties for the copper trace patterns.

The warpage predictions from these models are shown in Figure 3.3 for the exact model and Figure 3.4 for the effective isotropic property model. As seen in the figures, the warpage predictions from the two models differ significantly.

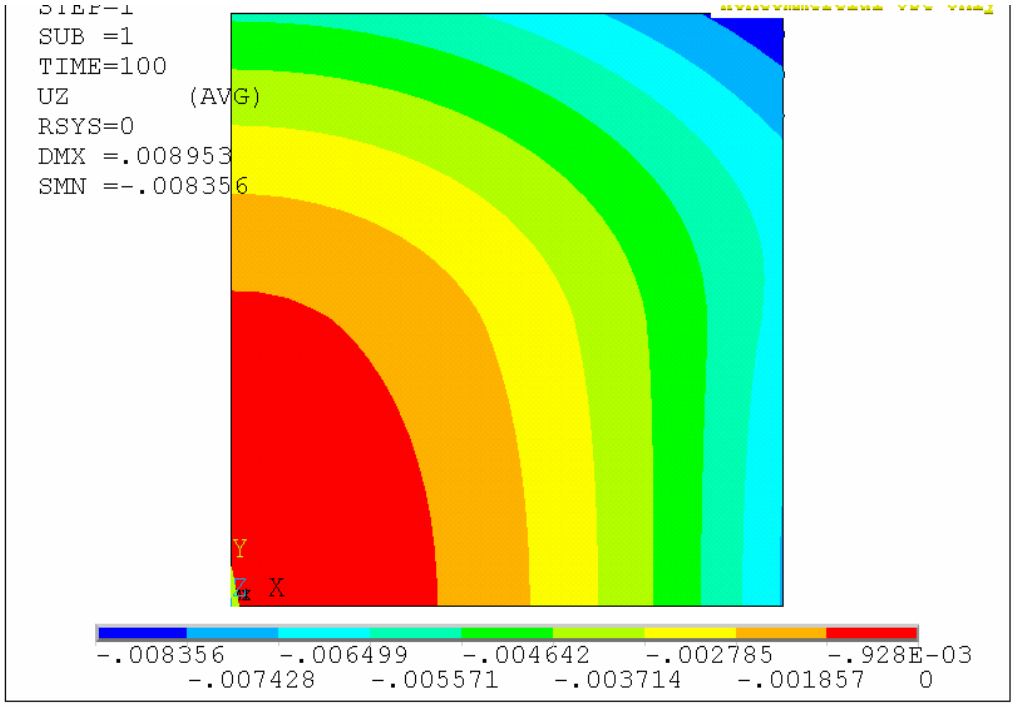

Figure 4.3: Warpage prediction from exact model for Figure 3.1

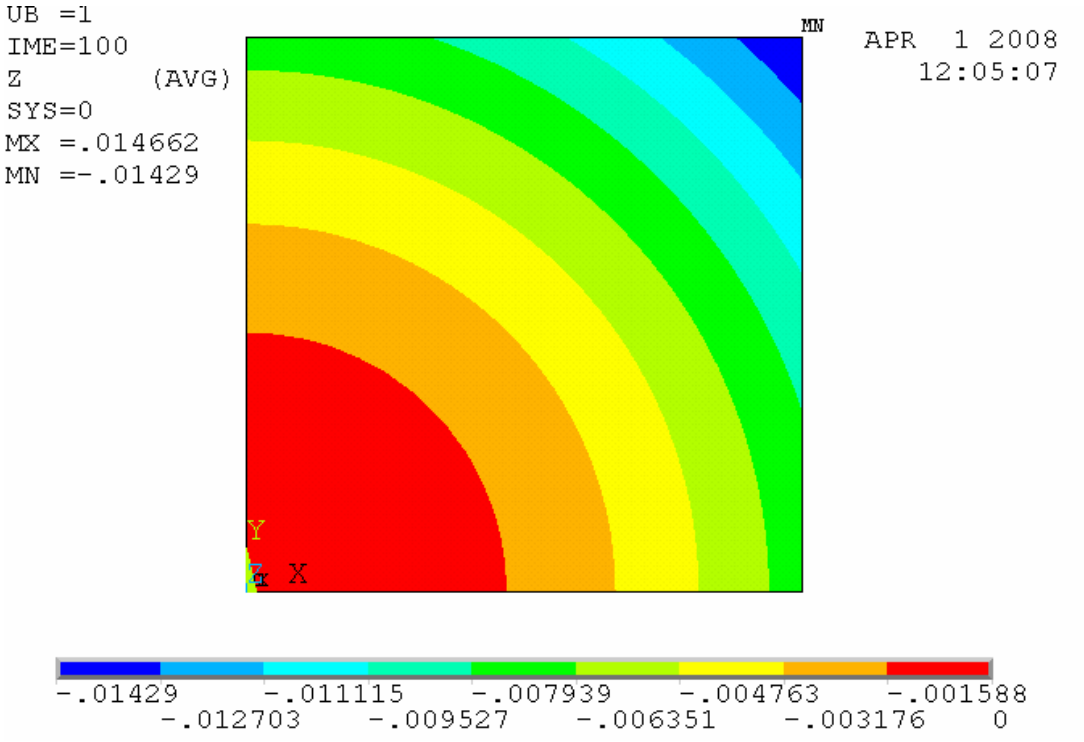

Figure 4.4: Warpage prediction from isotropic micromechanics approach for Figure 3.1

This analysis was repeated for a substrate with a trace pattern which had the areas of copper and dielectric material exchanged, as shown in Figure 3.5. The warpage prediction for this substrate is shown in Figure 3.6 for the exact model and in Figure 3.7 for the effective isotropic property model. As seen in the figures, the warpage predictions from these to models are also significantly different.

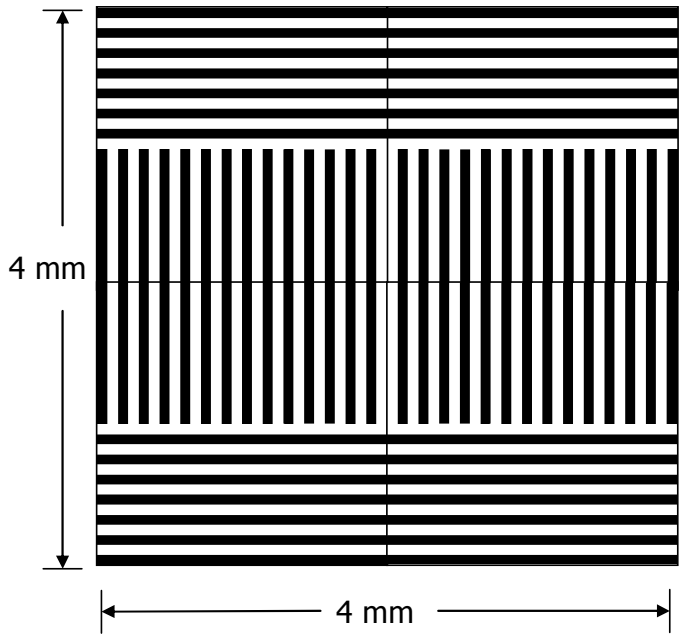

Figure 4.5: Alternative trace pattern modeled

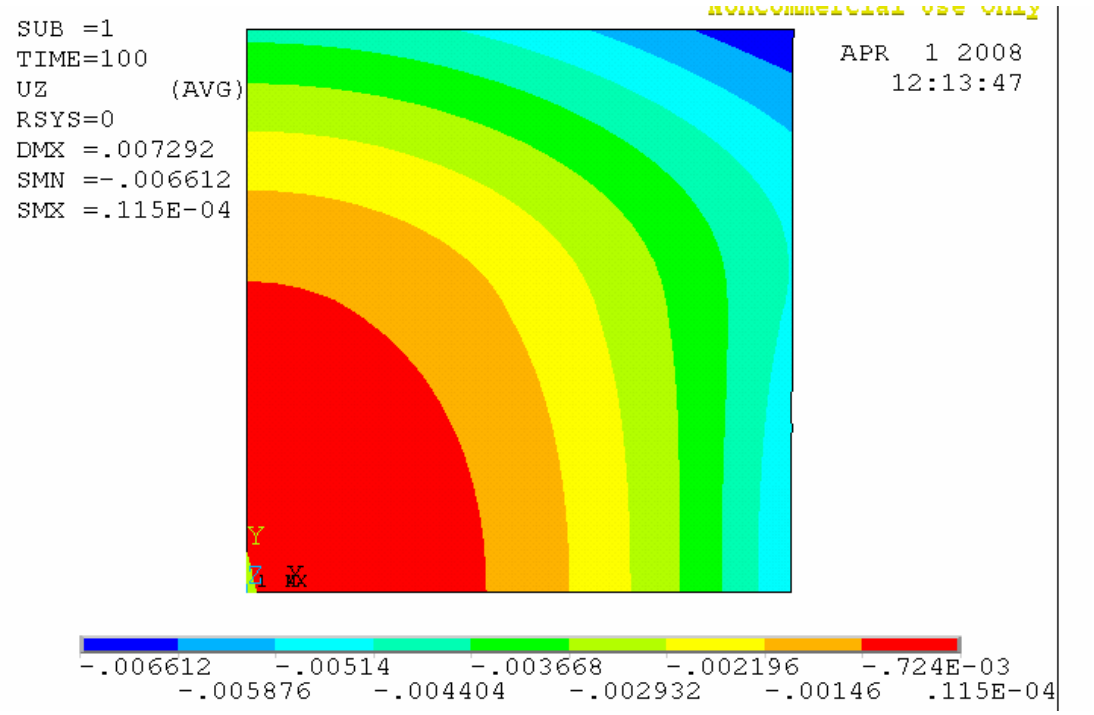

Figure 4.6: Warpage prediction from exact model for Figure 3.5

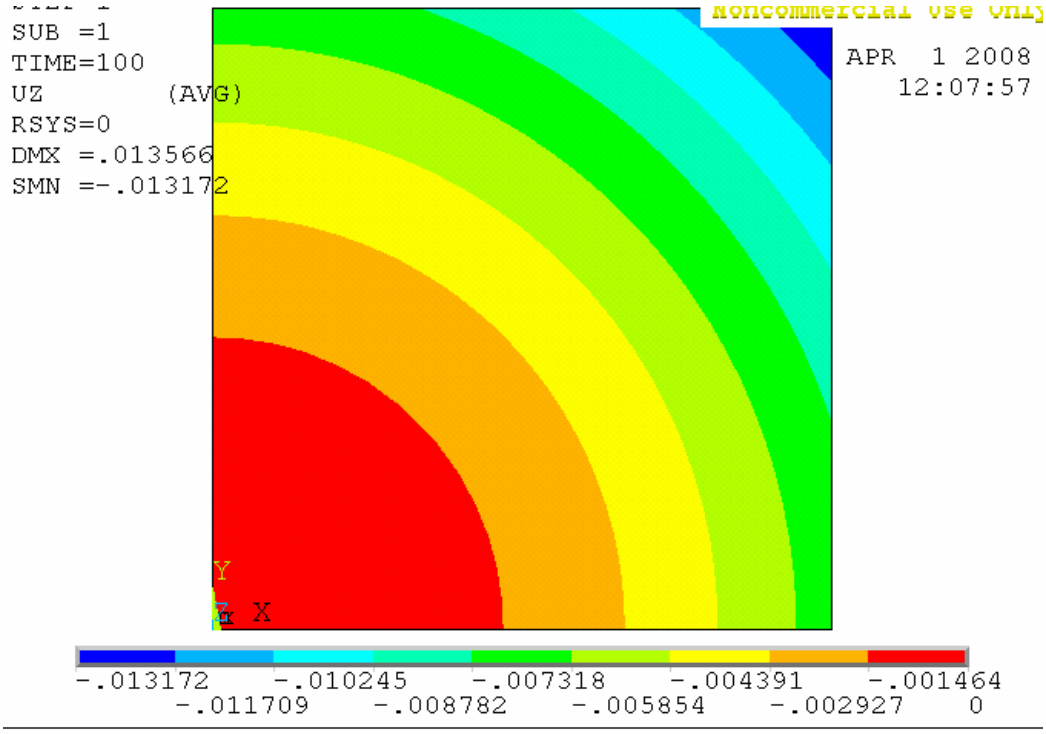

Figure 4.7: Warpage prediction from isotropic micromechanics approach for Figure 3.5

The difference in warpage predictions is probably so pronounced because the substrate modeled is very flexible and the trace pattern is in a coherent direction. The error in warpage prediction may not be as noticeable in stiffer substrates or in substrates with more randomized trace patterns. However, since flexible substrates are in demand, it is important to develop a methodology capable of accurately predicting warpage for them.

CHAPTER 5

METHODOLOGY TO ACCOUNT FOR COPPER TRACE PATTERN CHARACTERISTICS

To address the previously mentioned problems a new method was developed to calculate the material properties in mixed copper and dielectric layers. Since copper traces often run parallel to each other in a given small area of a trace pattern, the basis for this approach is to divide the trace pattern in a given substrate layer into small areas and find a way to calculate the average direction in which the traces in that area run. This average direction could be coupled with the previously mentioned micromechanics equations and a calculation of the percentage of copper in each small area to yield directional material properties for that area.

The first step of this analysis was to prepare a trace pattern image with all of the areas containing copper filled with one color and all the areas containing dielectric material left black. This image was then loaded into MATLAB. In MATLAB, image files are converted to a matrix of size $m \times n \times 3$ where m and n are the number of vertical and horizontal pixels and the three layers represent the colors red, green, and blue. The values of the matrix represent the intensity of each color in a given pixel. The color representing the trace pattern is then inferred by the developed program by calculating the average intensity of each color and selecting the color with the average highest intensity as that representing the trace pattern. One of the colors red, green, or blue is best used to represent the trace pattern, as this allows better accuracy in the calculation of which color represents the trace pattern, as well as the calculations in the following steps. After the color representing the trace pattern has been selected, the image is then subdivided into smaller areas for analysis in later steps.

5.1 Calculation of Copper Percentage in Small Areas

The calculation of the percentage of copper in each small area was a rather simple process for substrates with no holes in them. An image of the trace pattern was prepared and subdivided as described above. In each small area the number of colored pixels was counted along with the number of total pixels. The copper percentage was calculated as shown in Equation (4.1).

$$Copper\ \% = \frac{\#\ of\ ColoredPixels}{\#\ of\ TotalPixels} \tag{4.1}$$

If there is a hole in the substrate the procedure becomes slightly more complicated. Any holes in the substrate must be colored in with a color other than the color used to represent copper. Again, one of the colors red, green, or blue is best used for this. So if green were used to represent copper red could be used to represent a hole in the substrate. In this case the number of red pixels would also be counted and subtracted from the number of total pixels as shown in Equation (4.2)

$$Copper\ \% = \frac{\#\ of\ Green\ Pixels}{\#\ of\ Total\ Pixels - \#\ of\ Red\ Pixels} \tag{4.2}$$

This allows the copper percentage to be calculated without including the effects of the hole. The hole can then be modeled in the ANSYS geometry, which is a more accurate representation of it.

5.2 Calculation of Average Trace Direction

The calculation of the average direction of the traces in a given small area proved to be a more challenging task. The steps to do so are as follows. After the image is prepared as described above it is converted into a black and white image by creating a

new matrix with values equal to the most intense layer of the matrix representation of the original image. This image is then converted into a binary image consisting of the edges of the black and white representation by detecting large changes in intensity. Where there is a large change in intensity in the black and white image there is an edge. A Hough transform, which will be described later, can then be performed on this binary image to find lines. This process is demonstrated in Figure 5.1 for a small section of a trace pattern. The image in the top left shows a section of the original trace pattern image. The image in the top right shows the matrix representation of the image has been changed from $m \times n \times 3$ from $m \times n \times 1$. The bottom left shows the image after it has been converted to a binary image. Notice that only the edges show up in this representation. Finally, the image in the bottom right shows the lines which are detected by the Hough transform.

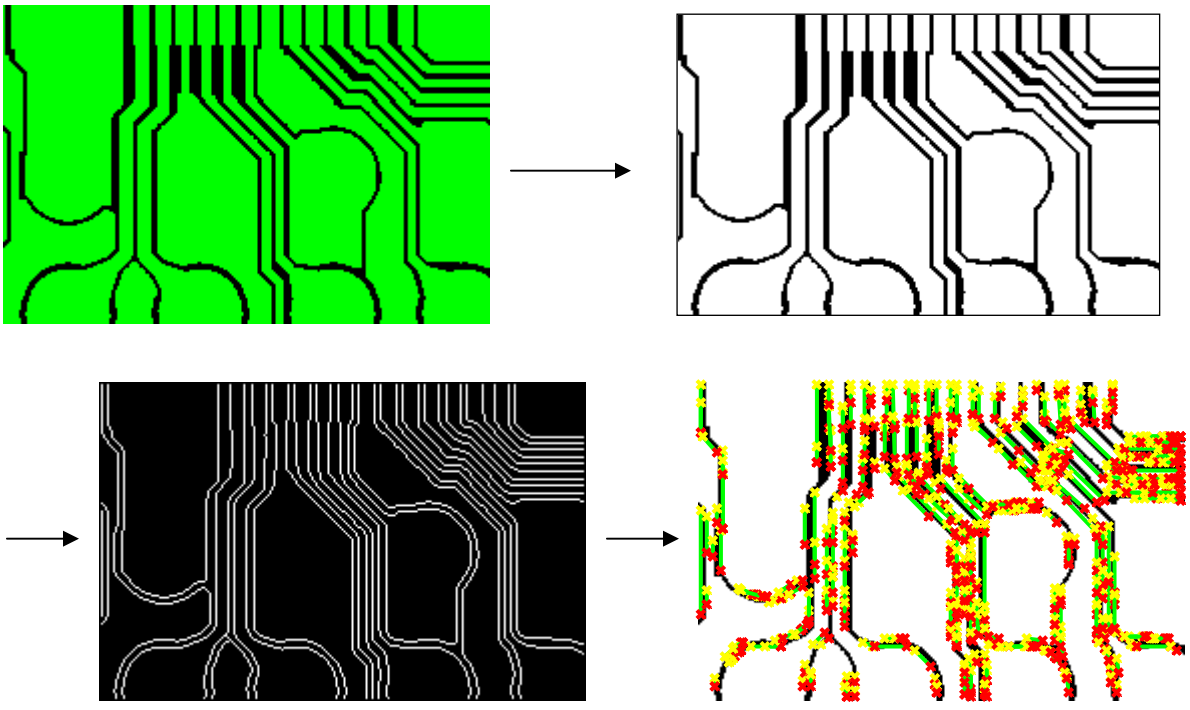

Figure 5.1: The steps required to calculate the lines in an image of a trace pattern.

The Hough transform is used to find lines in digital pictures. This method was first developed by Hough (1959) and expanded on by Duda and Hart (1972). This method works by first making a parameterized version of the digital image with the so called normal parameterization. In this parameterization scheme, lines are represented by Equation (4.3)

$$x\cos\theta + y\sin\theta = \rho \tag{4.3}$$

Where x and y are the coordinates of a point on the x-y plane and θ and ρ are the angle and distance of a line running from the origin and perpendicular to a given line drawn through the point *x, y*. Many lines are drawn through each point, and each line will have a unique θ and ρ, as shown in Figure 5.2.

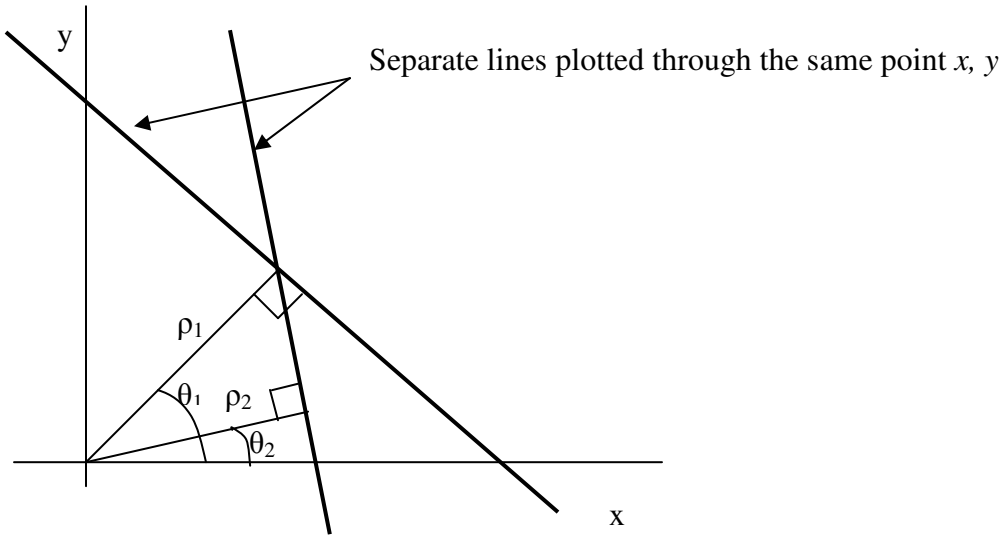

Figure 5.2: Normal parameters used to represent lines

In this parameterization every line on the *x-y* plane corresponds to a unique point on the θ-ρ plane. Also, any point in *x-y* will correspond to a sinusoidal curve in θ-ρ.

So any set of collinear points in *x*-*y* will form intersecting curves in θ - ρ . This is demonstrated in Figure 5.3.

In the top part of Figure 5.3, several lines are plotted through 3 data points. Bold lines are also plotted perpendicular to the lines running through the data points so that they intersect the origin. The length of each bold perpendicular line is the ρ for that line, and the angle it is drawn at is θ. A tabulated list of each ρ and θ is shown below each plot. If the possible ρ and θ values for each point are plotted in θ - ρ space, as in the lower half of the figure, the points can be joined to make a smooth sinusoidal curve. As seen in the figure, the curves all intersect at the common ρ and θ which all of the three collinear points share. This ρ and θ can be used to describe the line which runs through all three points.

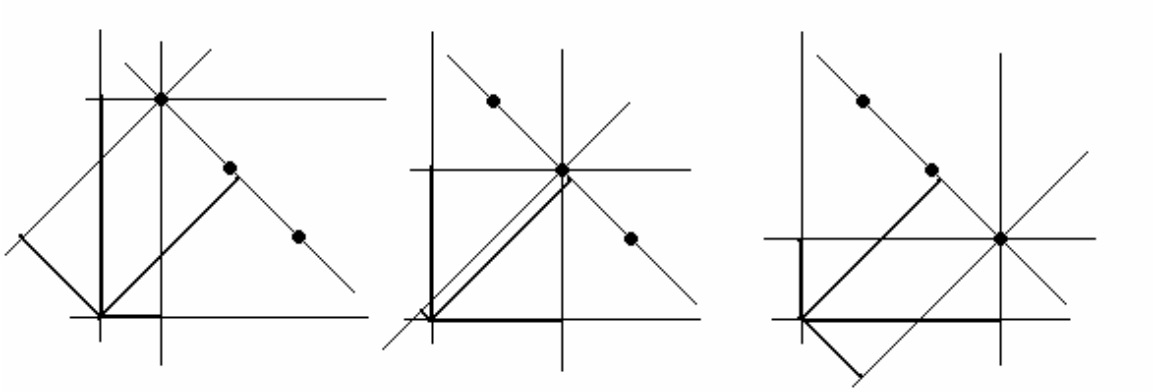

Theta	Rho
0	30
45	98.995
90	111
135	55.866

Theta	Rho
0	66.008
45	101.12
90	77
135	7.8102

Theta	Rho
0	101
45	101.12
90	42
135	41.725

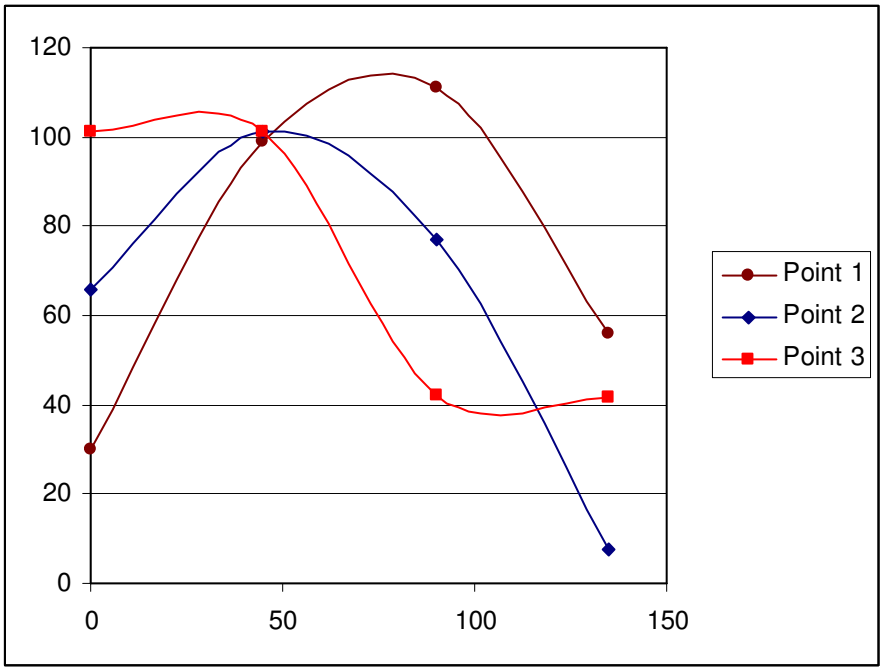

Figure 5.3: Demonstration of the Hough transform for three collinear points

With this in mind we can reason that a line in a digital image, being made up of many points, will appear as the intersection of a large number of curves in a Hough transform, as shown in Figure 5.4.

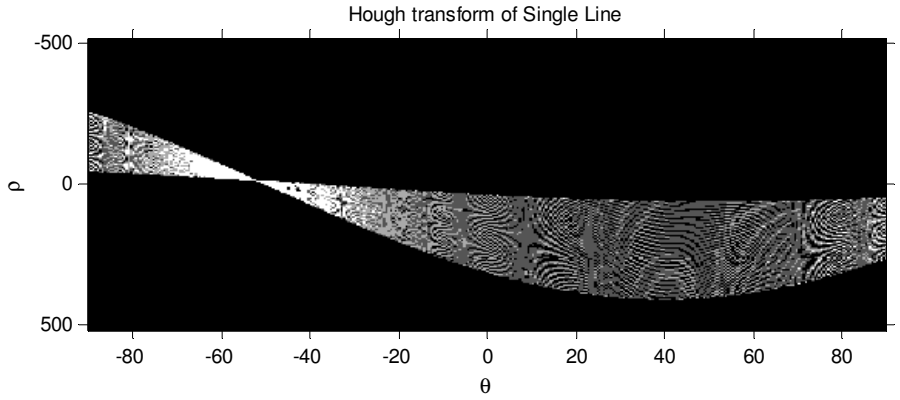

Figure 5.4: Hough transform of a single line

After the Hough transform has been performed the locations of the "peaks", or locations where a large number of curves intersect on the Hough transform plot can be analyzed to find out the slope and location of the lines in the input image, as shown in Figure 5.5. These peaks can be selected automatically by setting a threshold intensity above which a point will be selected as a peak. The sensitivity of the developed program to finding peaks can be adjusting by changing this threshold intensity. Setting the threshold too low will result in a large number of false positives, or locations where there are not really lines. Setting the threshold too high will result in too few lines being detected.

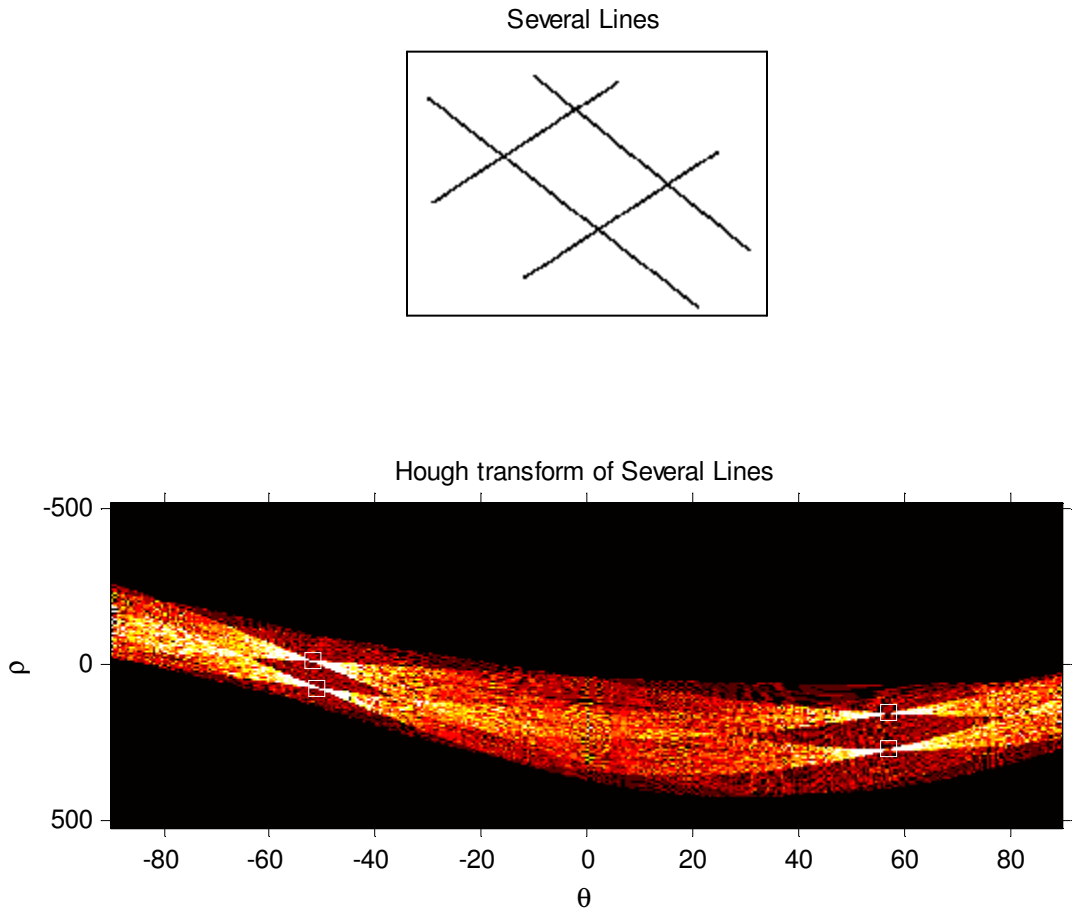

Figure 5.5: (Top) Several lines at different angles. (Bottom) Hough transfrom of the image above with the peaks boxed in.

When performed on even a small section of an image of a complicated trace pattern this operation will give locations for a large number of lines. The direction of an average line must then be calculated from this data.

The average line is calculated by first calculating the slope of each line detected by the Hough transform. The lines with positive and negative slopes are then grouped together and the average slope of each group is calculated. The two groups must be

analyzed separately, as positive and negative lines can cancel each other out when attempting to find their average, as demonstrated in Figure 5.6.

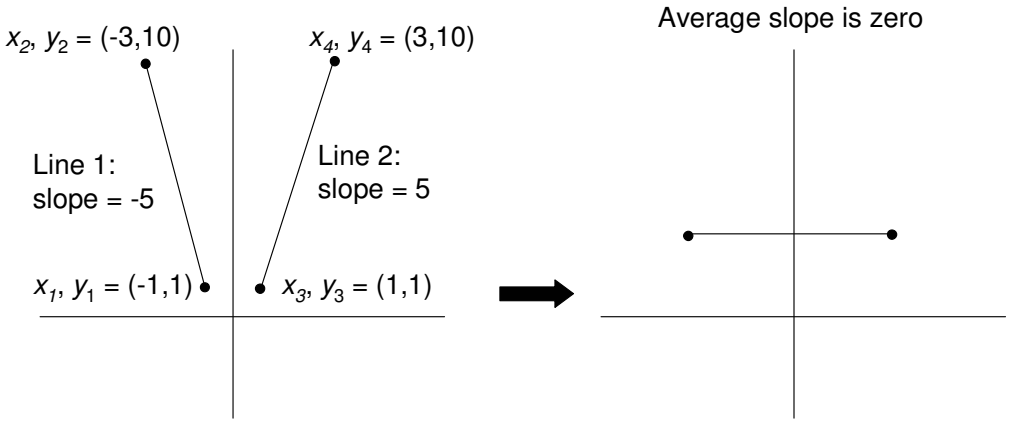

Figure 5.6: Demonstration of need to group lines into positive and negative slopes

The total length of all the lines with positive slopes and negative slopes is also calculated. This number will be used to decide which group of lines is more prevalent in the image and should therefore have the stronger effect on what the final average slope is. If the positive and negative slopes are both above or both below 45°, the average of the two lines is used. The way this average is calculated depends on the slopes. If the two slopes are both above 45°, the average is calculated so that the horizontal component cancels out. If the slopes are below 45°, the average is calculated so the vertical components cancel out. If the slopes of the average lines are on opposite sides of 45°, the set with the longer total length is used.

These calculation strategies are demonstrated in Figures 5.7, 5.8 and 5.9. In Figure 5.7, the positive and negative slopes are both above 45°. The length of the negative line is slightly longer than the length of the positive line. Therefore, since the final average line is a weighted average of the two it will appear as a line with a negative

slope which is steeper than the average negative line. In Figure 5.8, the average positive and negative lines have slopes of less than 45° and the average positive line has a slightly longer length. Therefore, the final average line will be a line with a positive slope which is somewhat less than the slope of the average positive line. In Figure 5.9, the average positive and negative lines have very different slopes, but the average positive line has a much longer length. Therefore, the average positive line is used for the final average line. If the two lines have very different slopes and are similar in length, isotropic properties are applied.

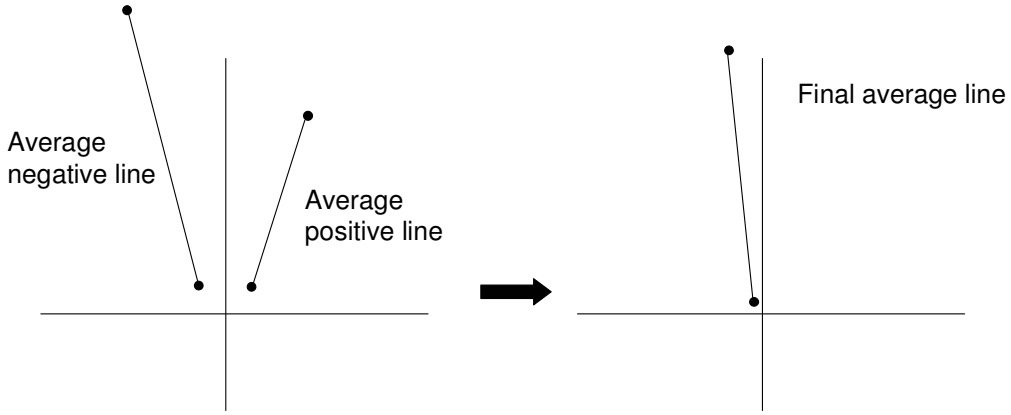

Figure 5.7: Calculation for two lines with steep slopes

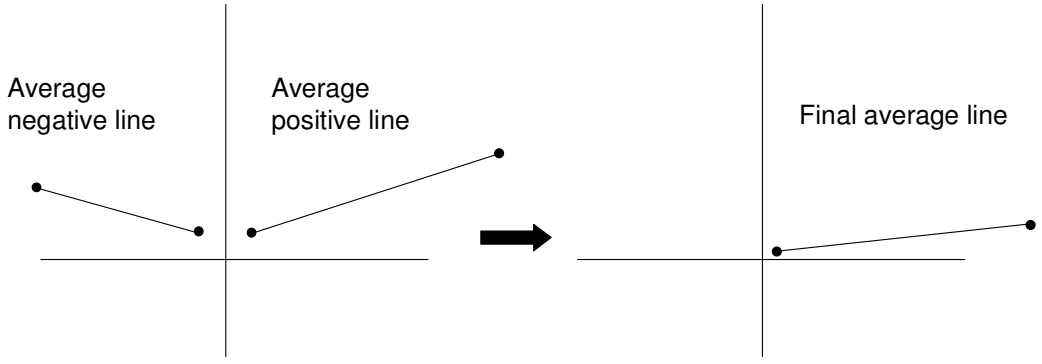

Figure 5.8: Calculation for two lines with shallow slopes

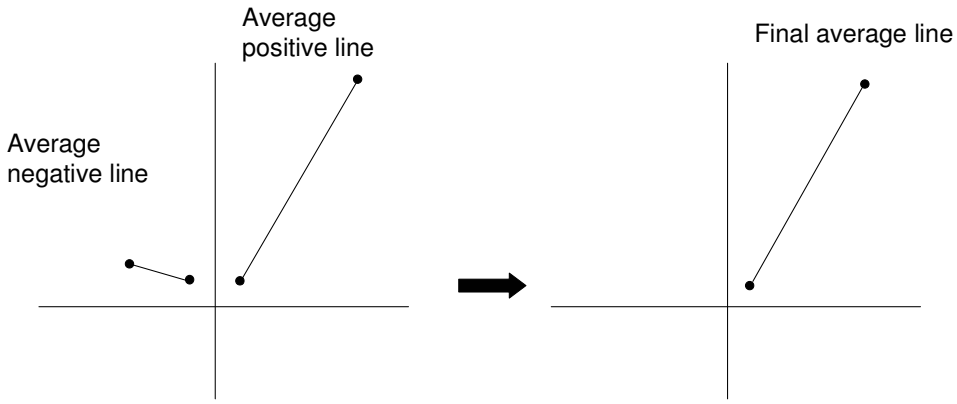

Figure 5.9: Calculation for average lines with largely different slopes

In this calculation method, horizontal and vertical lines can become a problem, as it is difficult to tell which group (positive or negative) to put them in. If there are a large number of horizontal or vertical lines in an image and they are all grouped with either the positive or negative lines the total length will be incorrectly represented, leading to incorrect weights being assigned to the average lines. For this reason horizontal and vertical lines are excluded from calculations of which slope is more prevalent in the image, however it is important that they are included in average slope calculations, as excluding them could significantly alter calculations if a large number of vertical or horizontal lines are present. For these calculations half of the horizontal and vertical lines contribute to the positive slope and half contribute to the negative slope, as it was found that allowing them to contribute fully to either would make the final calculation either too steep or too flat.

Some small areas do not have a well defined direction. A given area may not have enough lines in it for a well defined direction to be detected, or the trace pattern may have a crisscrossed pattern. The program can easily check to see that a minimum number of lines has been detected in each area. However, necessary to define some logic in the

program to decide weather or not a well defined direction existed if there were enough lines. If no well defined direction exists in a certain area of the trace pattern then isotropic properties can be applied.

The program decides if there is a well defined direction by first looking at the slopes of the average positive and negative lines. If the slopes of these lines are nearly perpendicular to each other it may be difficult to define a dominant direction. However, if there is a much larger number of positive lines or negative lines there may be a dominant direction despite this. Previously, the total length of the positive and negative lines was calculated. This calculation is now used to see if one of the sets is more prevalent. If one of the sets is more than 30% larger in total length, the average line associated with it is assumed to be the average direction of the area. If both sets are within 30% of each other in total length, isotropic properties are used as they are described in chapter 4. The cutoff was set at 30% based on empirical evidence. It was found by trial and error that length differences below 30% resulted in average lines being applied to some crisscrossed areas. Figure 5.10 shows a trace pattern which has a crisscrossed pattern. A trace pattern such as this would result in the average lines shown in Figure 5.11. This trace pattern was determined to have no dominant direction and isotropic properties would be applied to it for analysis.

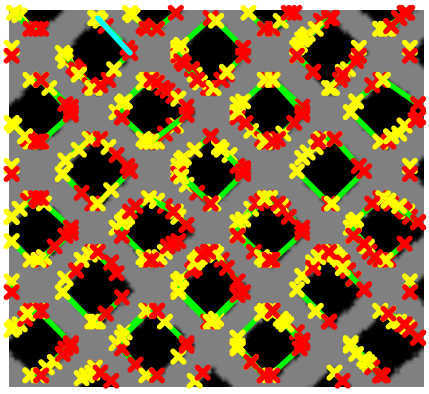

Figure 5.10: Trace pattern with no well defined direction

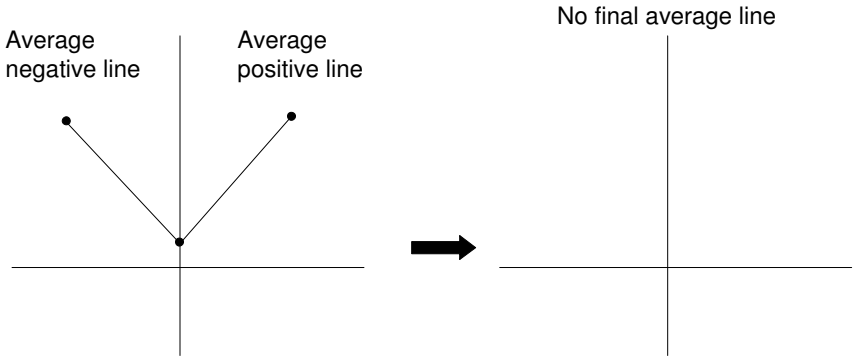

Figure 5.11: Average lines for crisscrossed pattern

5.3 Calculation of Material Properties

Once the average direction of traces in a small area has been calculated, micromechanics formulations can be used to obtain the effective material properties of that area. These equations are the same as Equations 4.1-3.8, and they are repeated here for easy reference.

$$E_{11} = E_f V_f + E_m V_m \tag{4.4}$$

$$E_{22} = \frac{E_f E_m}{E_f V_m + E_m V_f} \tag{4.5}$$

$$\nu_{12} = \nu_f V_f + \nu_m V_m \tag{4.6}$$

$$\nu_{21} = \frac{E_{22}}{E_{11}} \nu_{12} \tag{4.7}$$

$$\alpha_{11} = \frac{\alpha_f E_f V_f + \alpha_m E_m V_m}{E_f V_f + E_m V_m} \tag{4.8}$$

$$\alpha_{22} = (1+\nu_f)\alpha_f V_f + (1+\nu_m)\alpha_m V_m - \alpha_{11}\nu_{12} \tag{4.9}$$

$$G_{12} = \frac{G_f G_m}{G_f V_m + G_m V_f} \tag{4.10}$$

Where E = Young's modulus

υ = Poisson's ratio

α = CTE

G = Shear modulus

V = Volume fraction

f, m = Fiber and matrix directions (respectively)

11, 22, 12, 21 = Longitudinal, transverse, major, and minor directions

Note that no equations are given for material properties are given for E_{33}, α_{33}, G_{21}, and G_{23}. There was not found to be a consensus on what calculations to perform to obtain material properties in these directions. For this analysis, the properties were set to be those in the 22 direction or the 21 direction. Starting from this approximation a sensitivity analysis to properties in these directions was carried out. It was found that E_{33}, α_{33}, G_{21}, and G_{23} have a very small effect on warpage, with changes in each variable of 10% changing the warpage by less than .1%.

5.4 Application to Finite Element Models

Now that the average direction and material properties are known, they can be used to make FE models. When the average direction and material properties of all sections are calculated in MATLAB, they are saved as text arrays for importation into ANSYS. Once the arrays are imported into ANSYS they are used to build material models. One material model is made for each small section of each layer of a substrate, so for a substrate with 8 x 8 divisions and 5 mixed copper and dielectric layers there would be 140 material models. After the substrate geometry is constructed in ANSYS it is divided into areas equal in size to those in the MATLAB analysis. The areas are meshed using shell181 elements, as substrate layers are often thin and can be difficult to model with 3D elements. Different section properties are applied to each small section of the divided substrate, corresponding to the material properties and effective directions calculated in MATLAB. Shell181 elements also allow for the orientation of material properties in individual layers in different directions, so the material property directions are oriented in the directions calculated previously. This yields a model with the substrate divided up into areas which are the same as those in the MATLAB portion of the analysis with the same material properties and directions as those calculated.

CHAPTER 6

VALIDATION OF THE DEVELOPED MODELING METHODOLOGY

As this effective property calculation method had not previously been implemented, it was desired to find some way to validate this procedure. A combined modeling and experimental approach was used to determine if this method predicted material properties accurately. In one part of the validation, models were made of substrates with simple trace patterns both with exact 3D models and with the methodology described. In the next part of the validation, the warpage of actual substrates was calculated using the described methodology and compared to the actual warpage of the substrate.

6.1 Comparison of Exact Models to the Effective Property Calculation Method

In this step of the validation the warpage of several substrates with simple trace patterns was calculated using exact models and the results of these calculations were compared to those obtained by constructing models using the described methodology. The exact models were made with no approximations for the mixed copper and dielectric layers. Areas with copper were modeled with different elements than areas with dielectric. These models were all considered to have one metal layer, an FR-4 core and two solder resist layers, as illustrated in Figure 6.1. In this analysis, the solder resist will mix into the copper layer, so the copper layer properties will be calculated from the combination of copper and solder resist properties for the models made with the described methodology. The material thicknesses are shown below in Figure 6.1.

Layer	Dimension (mm)
Solder resist top	0.04
FR-4	0.15
Copper	0.018
Solder resist bottom	0.03

Figure 6.1: Test substrate dimensions and stackup

The material properties for the materials in these simulations are shown in Tables 6.1-3

Table 6.1: Material properties for FR4 (Courtesy of Samsung Techwin)

MECHANICAL		THERMAL	
Young's Modulus	-	Density (kg/m^3)	193
Shear Modulus: G_{xz} (MPa)	693	Specific heat, c_p (J/kgK)	840
Shear Modulus: G_{xz} , G_{yz} (MPa)	199	Thermal Conductivity, κ (W/mK)	0.157
Poisson ratio: ν_{xz}	0.02		
Poisson ratio: ν_{xy}, ν_{yz}	0.1425		
CTE: α'_x,(ppm/K)	11.82		
CTE: α'_z (ppm/K)	13.34		
CTE: α'_y (ppm/K)	60.4 ($T<T_g$) 290 ($T>T_g$)		

Temp (°C) / Modulus	0	50	100	150
E_x (GPa)	19.01	16.97	15.17	13.22
E_z (GPa)	15.65	13.73	11.95	9.83
E_y (GPa)	1.625	1.600	1.575	1.550

Table 6.2: Material properties for copper (Polsky, 1998)

MECHANICAL		THERMAL	
Young's Modulus (GPa)	103.42	Density (kg/m^3)	8940
Poisson ratio	0.34	Specific heat, c_p (J/kgK)	384
Ultimate tensile strength, σ_{ult} (MPa)	275.8	Thermal Conductivity, κ (W/mK)	398
Yield stress, σ_y (MPa)	172.38		
CTE (ppm/K)	17.0		
Elongation at break (%)	12.0		

Table 6.3: Material properties for solder resist (Wong and Moon, Georgia Tech MSE Dept)

MECHANICAL							
Temperature (°C)		25	80	100	110	120	175
Young's Modulus (Mpa)		2412	1585	577	230	112	44
Poisson's Ratio	0.3						
CTE (ppm/K)	60						

In the manufacturing process, warpage is induced as the temperature the substrate is subjected to is lowered after the dielectric is cured. Therefore, for this analysis the

substrate is taken from a typical dielectric cure temperature of 150°C to room temperature, or 25°C.

The trace pattern of the first substrate analyzed is shown below in Figure 6.2. In this image, white represents copper trace areas and black represents solder resist areas. Note that the substrate has quarter symmetry. The models which were constructed took advantage of this feature by modeling the substrates with quarter symmetric boundary conditions. The models were made of the upper right quarter of the substrate. For quarter symmetry, motion in *y* and rotation about *x* are constrained along the lower side of the quarter modeled and motion in *x* and rotation about *y* are constrained along the left side. Additionally, the model is constrained in all degrees of freedom at one node on the lower left side of the model to prevent rigid body motion. The boundary conditions for the models are also shown in Figure 6.2.

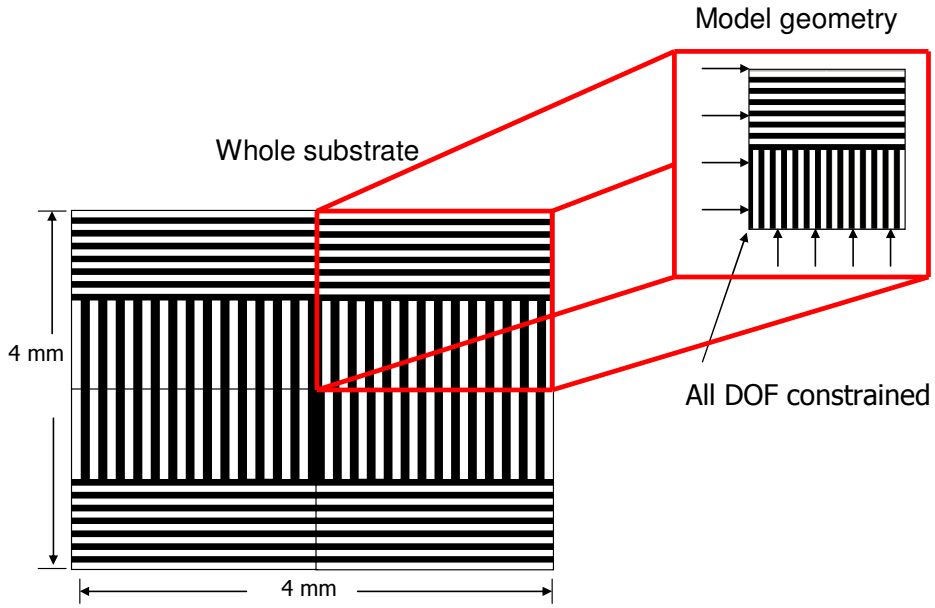

Figure 6.2: Trace pattern and boundary conditions for the first substrate analyzed for validation

Since only a quarter of the substrate was modeled, only the modeled portion needed to be analyzed in MATLAB and ANSYS. This portion of the pattern was divided into a 2*x*2 set of areas in MATLAB and ANSYS. The graphical output from MATLAB is shown in Figure 6.3. As shown by the figure, the program predicts that the lines will be either horizontal or vertical, which is obviously true by observation.

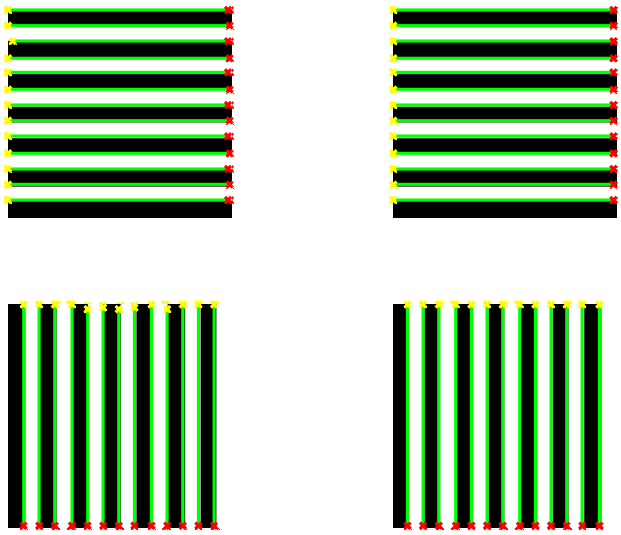

Figure 6.3: Output of Matlab program

The copper percentage was also calculated for each small area and the orthotropic properties of these sections were then calculated in MATLAB using Equations 5.4- 5.10. These properties were then imported into ANSYS to be used in the calculation of the warpage of the substrate with this trace pattern. The warpage prediction from the exact model of this substrate is shown in Figure 6.4 and the warpage prediction from a calculation performed using the described methodology is shown in Figure 6.5.

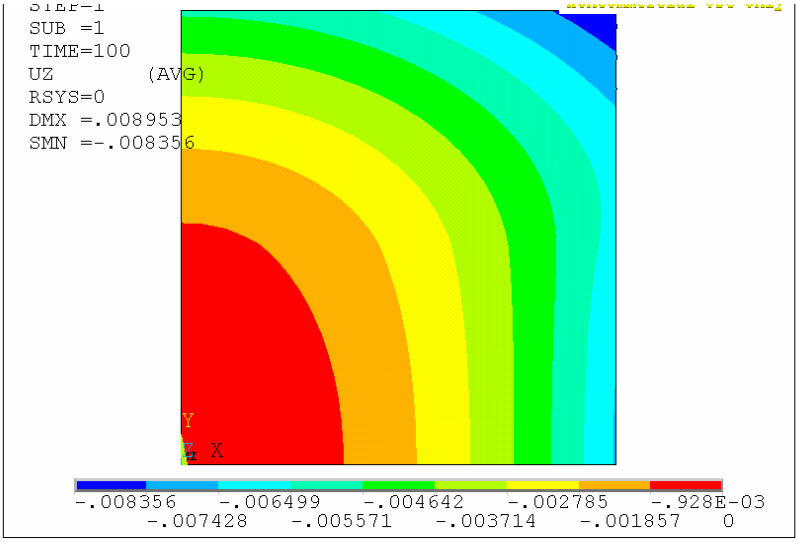

Figure 6.4: Warpage prediction from the exact model of the substrate shown in Figure 6.2

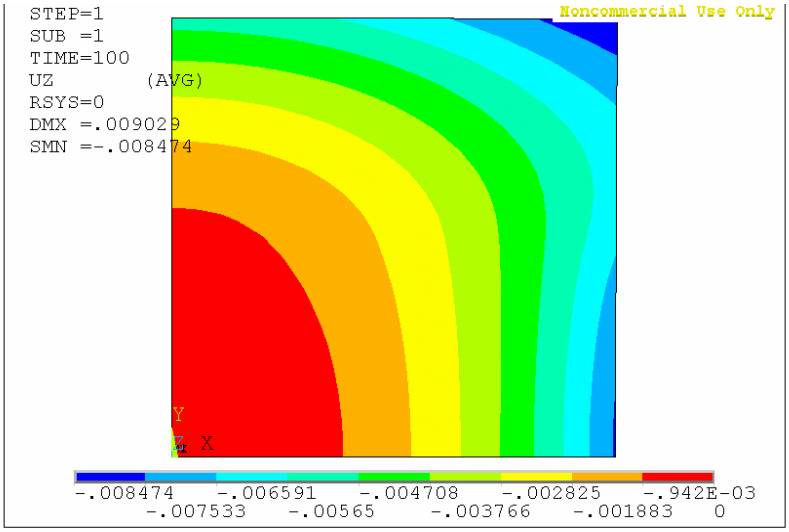

Figure 6.5: Warpage prediction from the developed effective property model for the substrate shown in Figure 6.2

Comparison of the results of the two models shows that the effective property calculation is very accurate. The warpage predictions from these calculations can be compared against the warpage prediction for the same substrate which was presented in Chapter 4. The prediction in Chapter 4 was calculated using only isotropic property

equations to calculate the effective material properties of mixed copper and solder resist layers. The warpage prediction for this substrate is repeated here in Figure 6.6 for easy reference. Notice that the prediction from the developed effective orthotropic property model is much closer to the prediction from the exact model than the prediction from the isotropic model. This indicates that the developed effective property model is more accurate than the previous isotropic model.

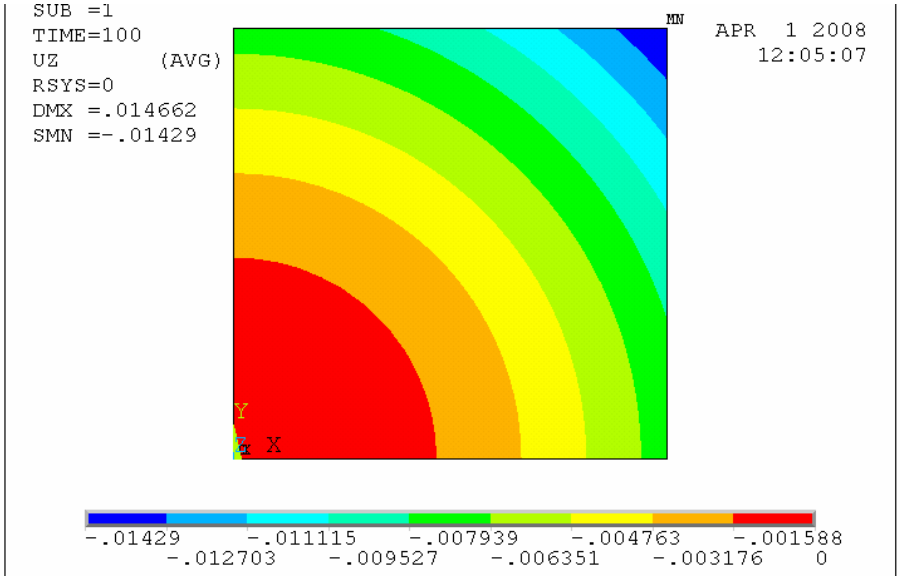

Figure 6.6: Warpage prediction for the substrate shown in Figure 6.2 modeled using only isotropic properties

As another test, this modeling methodology was carried out again for a substrate with the exact opposite trace pattern than the one previously analyzed. This pattern is shown in Figure 6.7. This substrate had the same material stack-up as the previous substrate and was constructed of the same materials. Again, an exact model was made with different elements used to represent the copper and solder resist areas and an effective property model was made using the developed methodology. Since the substrate

was still quarter symmetric, the same boundary conditions were used to construct its models as were used for the last set of models.

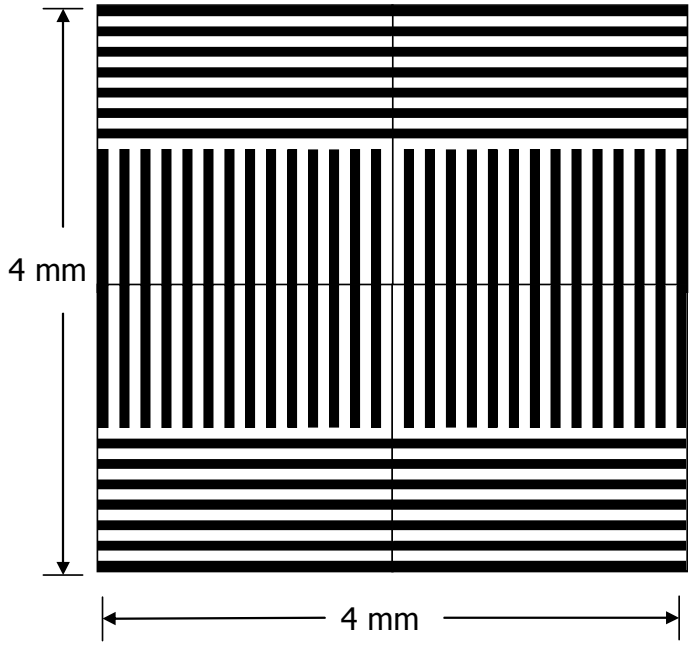

Figure 6.7: Trace pattern and geometry of alternate substrate tested

The warpage predictions from the exact model and the developed effective property model are shown in Figures 6.8 and 6.9 respectively. Inspection of the two figures shows that the warpage predictions from the exact model and the developed effective property model agree well. These models can also be compared to the model which was made of the same substrate but used only isotropic properties to calculate effective material properties in Chapter 4. This warpage prediction is also presented here in Figure 6.10 for ease of comparison.

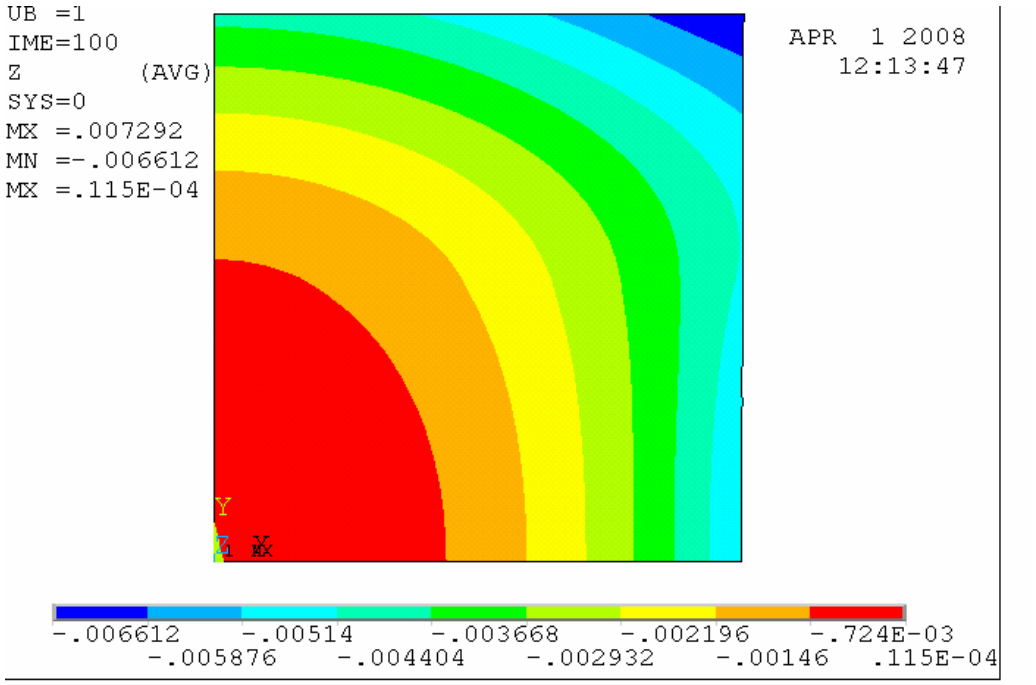

Figure 6.8: Warpage prediction from the exact model of a substrate with the trace pattern shown in figure 6.6

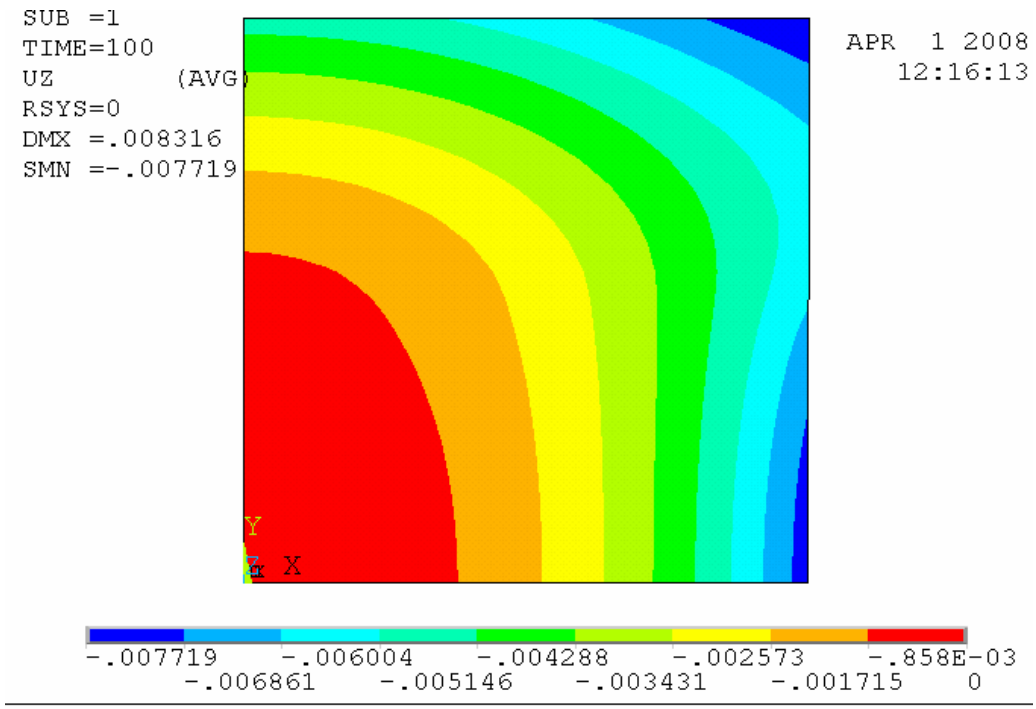

Figure 6.9: Warpage prediction from the developed effective property model for a substrate with the trace pattern shown in Figure 6.6.

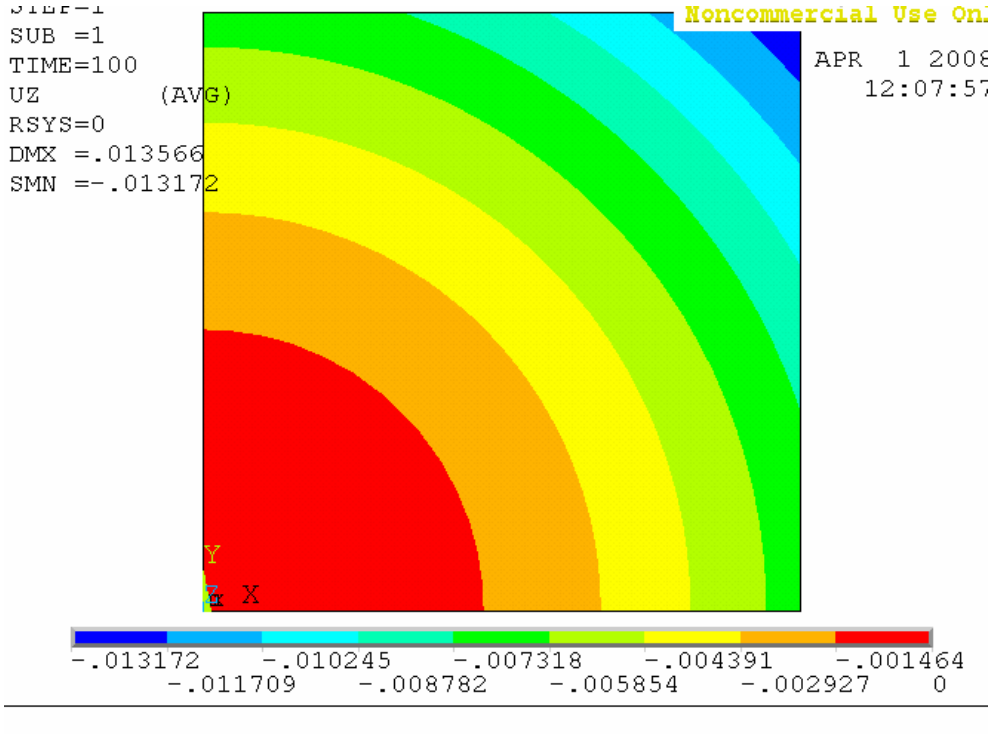

Figure 6.10: Warpage prediction from the isotropic effective property model presented in Chapter 4 for the substrate shown in Figure 6.6

Inspection of Figures 6.8 – 6.10 shows that the warpage prediction from the developed effective property model is in much closer agreement to that of the exact model than that of the isotropic effective property model.

As these models both have very simple trace patterns, the fact that the MATLAB program was able to calculate the average directions of the traces was unimpressive. Therefore, a substrate with the trace pattern shown in Figure 6.11 was modeled in ANSYS. As in the previous two cases, two analogous models were made, one using the exact trace pattern and the other using the developed methodology. This trace pattern is a small part of a commercial trace pattern. As it is complicated, an exact model in ANSYS was difficult to construct. However it was possible to import this trace pattern into ANSYS by means of the program LinkCAD, which is a program built for importing trace

patterns into ANSYS. Only a small section of the trace pattern could be modeled, since modeling the whole trace pattern takes far too many elements and too much processing time. This substrate also exhibits quarter symmetry, so the boundary conditions which were applied to the previous models will also be applied to the exact and effective property models made of this substrate.

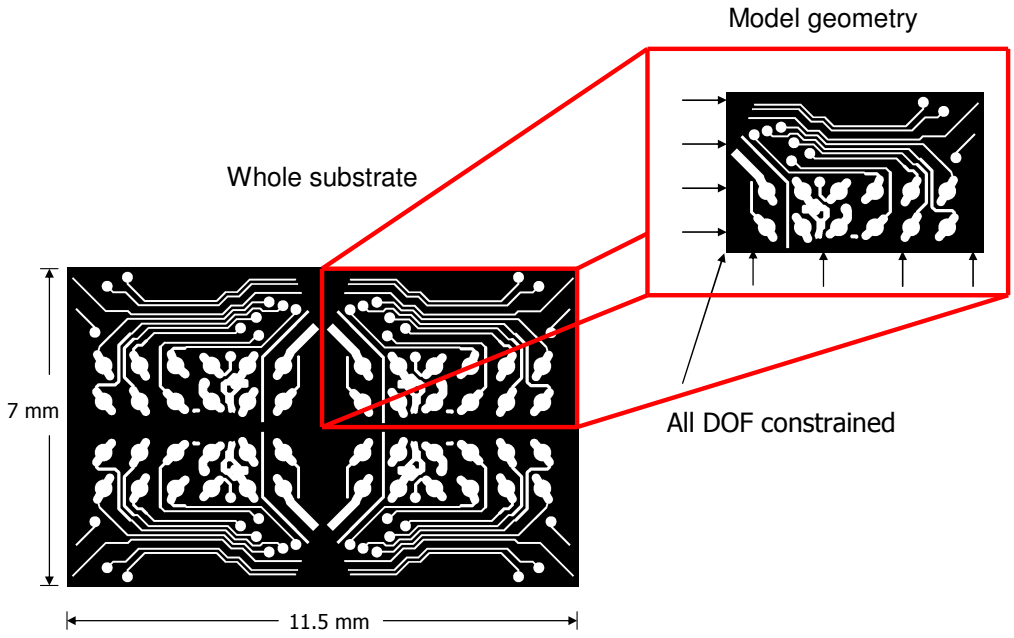

Figure 6.11: Small section of a commercial trace pattern modeled in ANSYS

As with the trace patterns of the two previous substrates, this pattern was first analyzed with the MATLAB program. The modeled area of the substrate was divided into 2*x*2 small areas. The resulting graphical output is shown in Figure 6.12. The blue lines in the images in Figure 6.12 represent the calculated effective direction of the traces in each small area. The effective orthotropic properties in each small area were calculated and these properties were then applied to the effective property model.

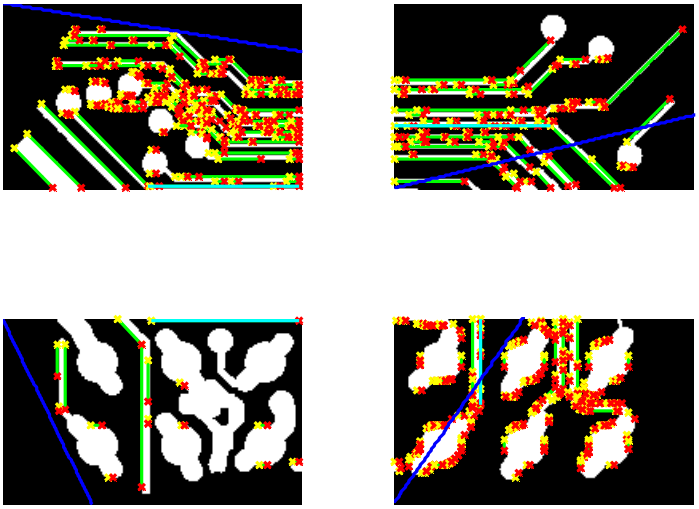

Figure 6.12: Graphical output from matlab program

The warpage prediction from the exact model is shown in Figure 6.11 and the prediction from the developed effective property model is shown Figure 6.12.

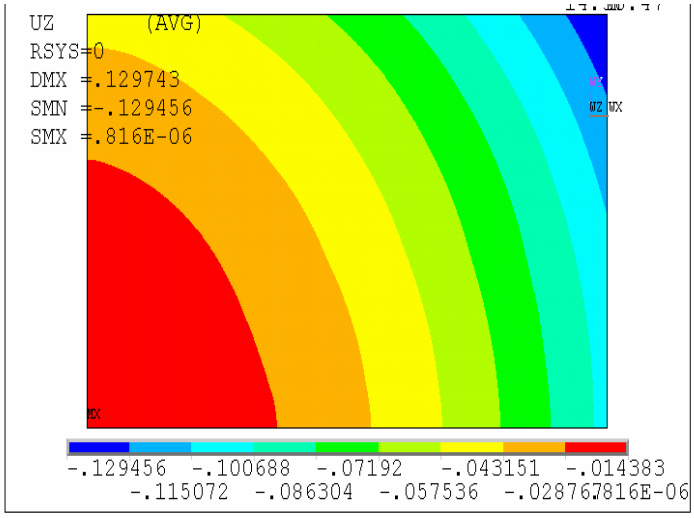

Figure 6.13: Warpage prediction from exact model for a substrate with thetrace pattern shown in Figure 6.11

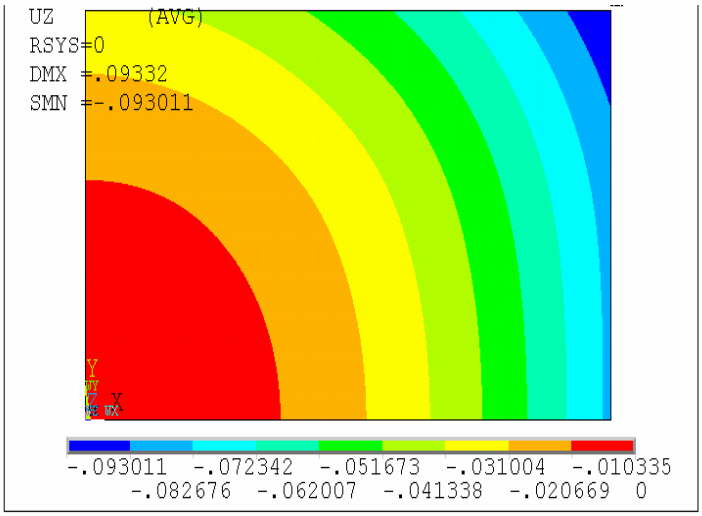

Figure 6.14: Warpage prediction from effective property model for a substrate with the trace pattern shown in Figure 6.9

Inspection of the figures shows that the warpage prediction from the developed effective property model closely matches the warpage prediction from the exact model. As these modeling attempts showed good results, it was desired to go on to the next step of comparing warpage predictions from the developed effective property model to experimentally measured warpage of actual substrates.

6.2 Comparison of Effective Property Models to Experimental Results

The previous section was useful as it provided validation without having to obtain experimental data. However, it was also desired to show that this method will predict the warpage of an actual substrate. The substrate shown in Figure 6.15 was used to validate the developed effective property calculation method. The substrate is made up of blocks of a repeated pattern. Each repeated unit represents the substrate for a single chip. The chip will be attached to one side of the substrate and wire bonded to connections in the substrate. Solder balls will be attached to the other side of the substrate for connections to

the rest of the board. After the manufacturing process the substrate will be diced into individual packages.

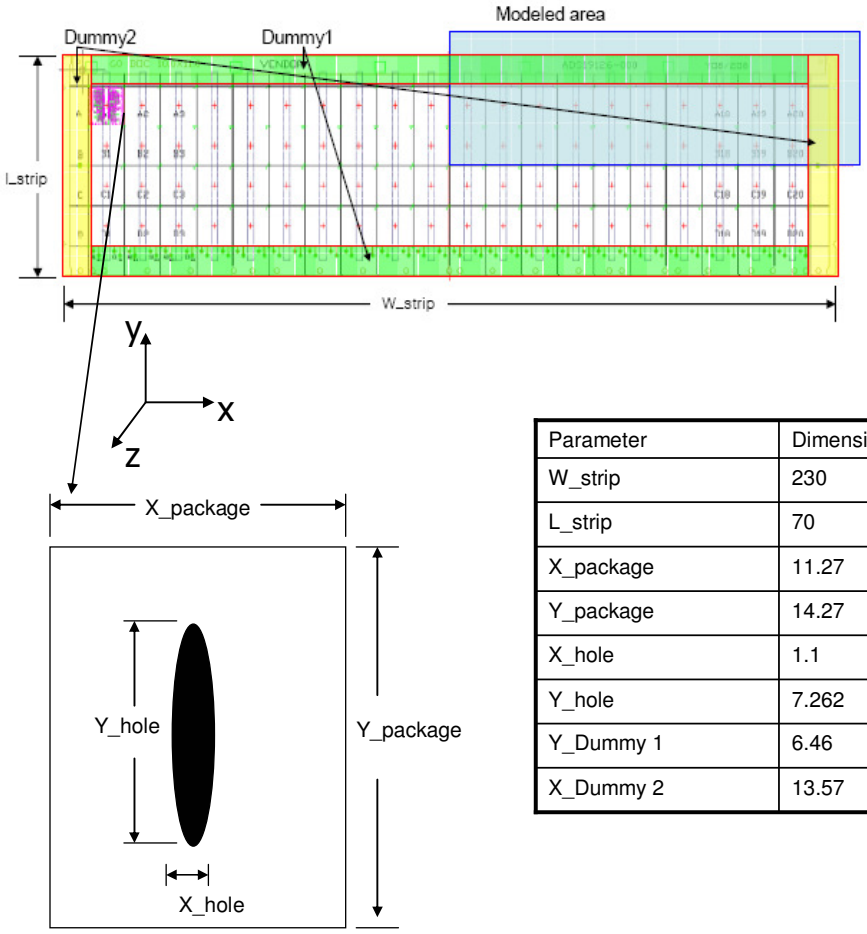

Parameter	Dimension (mm)
W_strip	230
L_strip	70
X_package	11.27
Y_package	14.27
X_hole	1.1
Y_hole	7.262
Y_Dummy 1	6.46
X_Dummy 2	13.57

Figure 6.15: Substrate modeled for experimental validation

The material properties in this substrate are the same as those listed in Tables 6.1-3. The material stack-up is shown in Figure 6.16. As seen in Figure 6.16, the substrate has an FR4 core, two metal layers, and two solder resist layers. When the solder resist is applied it will fill the gaps in the copper trace pattern, so effective orthotropic properties must be found for both metal layers.

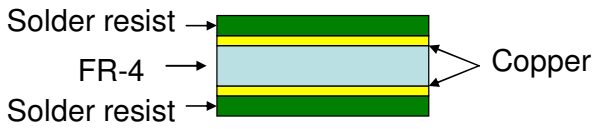

Layer	Dimension (mm)
FR-4	.15
Copper (Both layers)	.018
Solder resist (Both layers)	.03

Figure 6.16: Material stackup for substrate modeled in experimental validation

The experimental warpage was measured after the substrates had been baked for one hour at 175°C to remove moisture from them. Since this temperature is above the T_g of the solder resist material, the stresses in the solder resist material would be relieved at this temperature. Therefore, the solder resist was modeled as stress free at 175°C. Copper and FR-4 were taken to be stress free at 55°C, a common electroplating temperature.

The experimental warpage was measured with the substrate lying on a flat plate. Since this substrate is flexible, gravity has a significant effect on the measured warpage. To account for gravitational effects the substrate was modeled in a contact problem as laying against a rigid flat plate with a gravity load applied to it. The substrate was modeled both as a quarter model, with the upper right hand side modeled, as shown in Figure 6.15, and as a half model, with the entire right half modeled.

6.2.1 Trace Pattern and Division Size Analysis

The first step in the analysis of this substrate was to find the effective material properties from the trace pattern in each layer. Since the trace pattern was a repeated unit, only the trace pattern from one unit needed to be analyzed. The repeated units of the trace patterns in the two metal layers of the substrate are shown in Figure 6.17. The pattern on the left is for the ball attach side of the substrate and the pattern on the right is for the chip attach side of the substrate. Since many substrates, including this one, are multilayered, the MATLAB program was constructed to analyze all layers of a multilayer substrate in a single run.

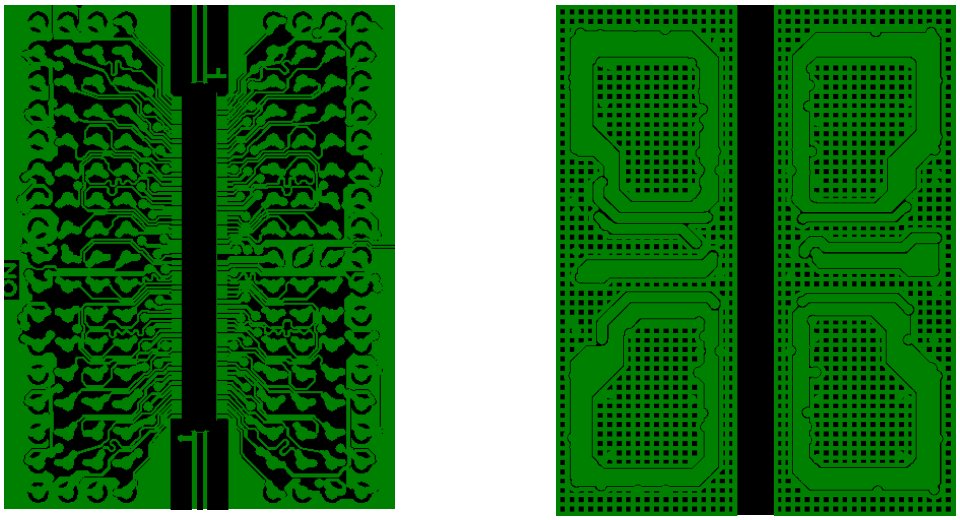

Figure 6.17: The repeated unit of the trace pattern in the metal layers of this substrate.

Notice that the trace pattern for the chip attach side is mostly a crisscrossed network. This means that the program should choose to fit isotropic properties to areas where this is the case. The visual output from the MATLAB program using 4 divisions in each direction for these trace patterns is shown in Figure 6.18. Inspection of this Figure shows that areas with crisscrossed patterns are generally identified as isotropic. The

MATLAB program was also run with 8 divisions in each direction. The output from this analysis is shown in Figure 6.19

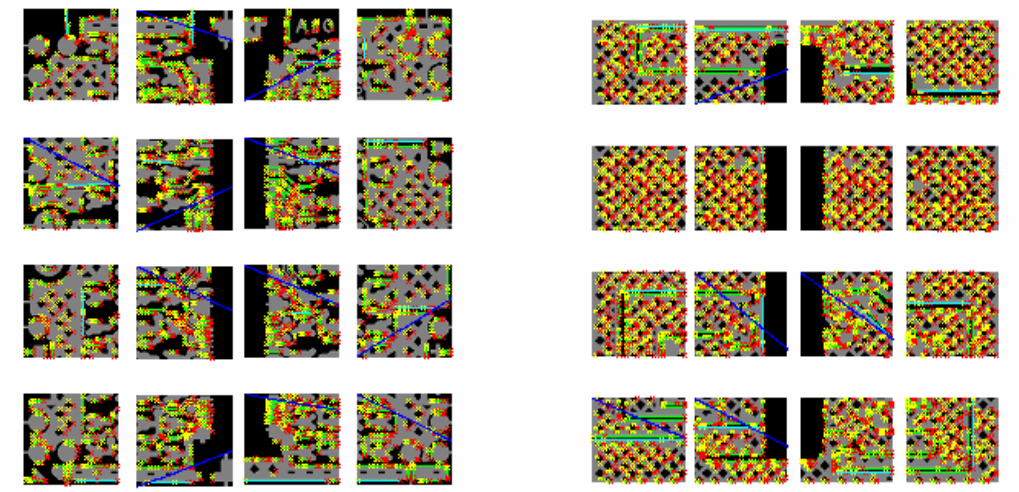

Figure 6.18: Effective trace orientations for 4*x*4 divisions the ball attach side is on the right and the chip attach on the left

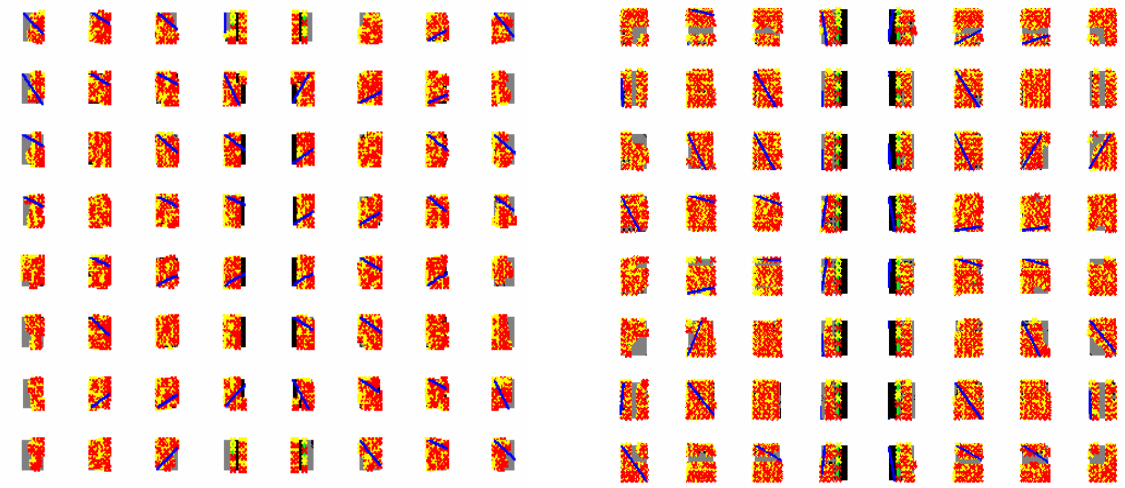

Figure 6.19: Effective trace orientations for 8x8 divisions the ball attach side is on the right and the chip attach on the left

As seen in the plots, many of the areas on the chip attach side do not show a dominant direction, especially in the 4*x*4 division plot. In the 8*x*8 division plot more effective directions could be found. This gives some evidence that the program is choosing the correct areas to define as isotropic. With this step in the analysis completed, the calculated properties and directions can be applied to a finite element model.

6.2.2 Modeling and Results

As stated, this substrate was modeled with both a quarter model and a half model. A quarter model was made first as the substrate is nearly quarter symmetric so implementing a quarter model would give a good approximation of the warpage. A half model was also made so that the difference between the half model and quarter model for this substrate could be observed. For the quarter model, the upper right hand side of the substrate was modeled, as shown in Figure 6.15. For the half model, the entire right hand side was modeled. The models were constructed with the ball attach side facing up.

The boundary conditions for the quarter model are:

1. M_x, $U_y = 0$ on the bottom side
2. M_y, $U_x = 0$ on the left side
3. All DOF = 0 on the bottom left node

The boundary conditions for the half model are:

1. M_y, $U_x = 0$ on the left side
2. All DOF = 0 at x, y = 0

As stated previously, the substrate in the ANSYS model was divided up into the same areas as in the MATLAB analysis. This means that each of the units of the substrate

was divided into 16 areas for the 4*x*4 division model and 64 areas for the 8*x*8 division model. Images of the area divisions for the 4*x*4 and 8*x*8 models can be seen in Figures 6.20 and 6.21. As seen in the figures, there are repeated units for each trace pattern which are equivalent to those used in the MATLAB analysis.

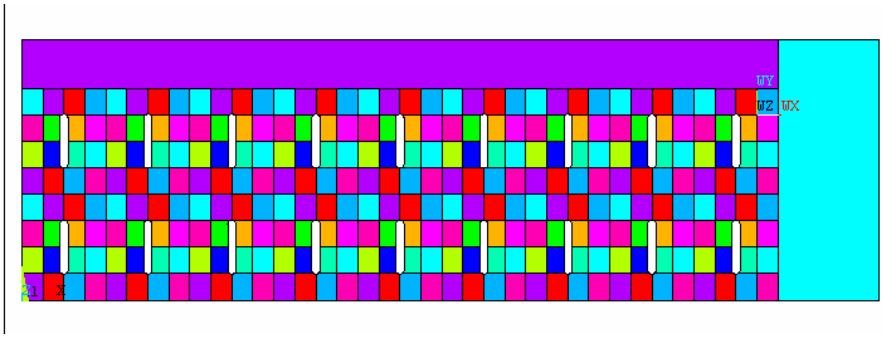

Figure 6.20: Area divisions in 4*x*4 division model

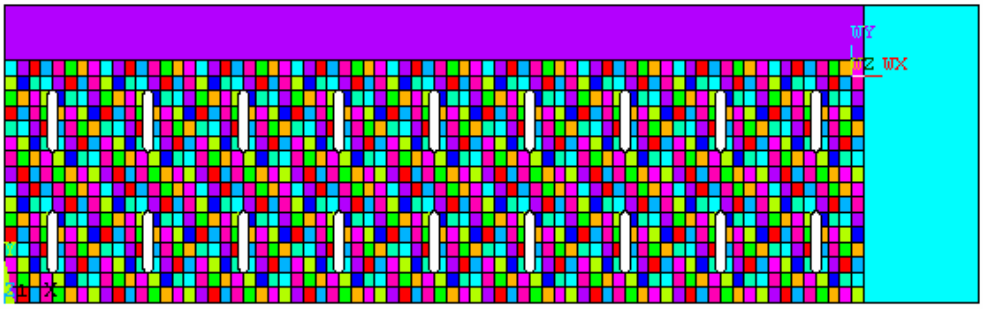

Figure 6.21: Area divisions for 8*x*8 division model

Meshing of the model was simplified by the process of dividing the model into small areas. Each small area could have the appropriate properties applied and then be free meshed. Using an element size of .5 provided a mesh with good element shapes. A picture of the mesh used is shown in Figure 6.22 for the 4*x*4 division model and in Figure 6.23 for the 8*x*8 division model.

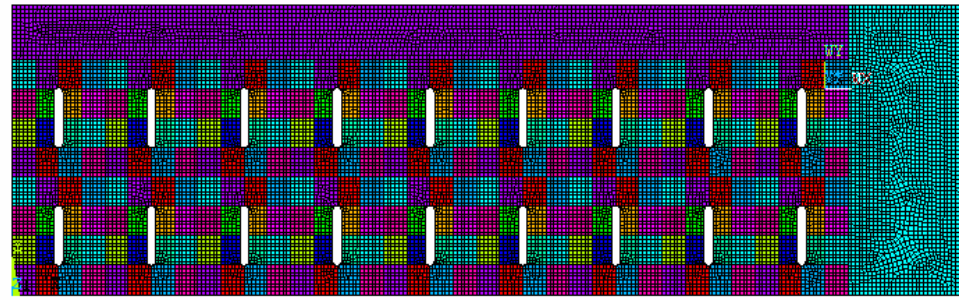

Figure 6.22: Mesh used in 4*x*4 division model

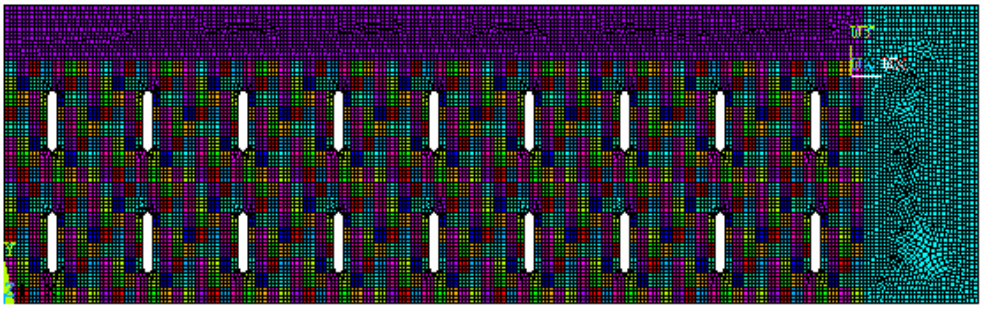

Figure 6.23: Mesh for 8*x*8 division model

The experimental warpage of these substrates was measured by laying the substrate on a flat surface and using shadow Moiré to measure the warpage. Since this substrate is very flexible, gravity will have a large effect on the measured warpage in a measurement system such as this. To account for gravity, an acceleration of 9.81 m/s^2 was applied in the negative z direction. Since the substrate was flat on a table, it was modeled as being in contact with a rigid flat plate which was held fixed at $z = 0$. The flat plate can be seen in the background of the modeling results.

After these steps the warpage prediction from the model could be obtained. The warpage prediction under the described conditions using the developed effective property model is shown below in Figure 6.24 without gravity applied and in Figure 6.25 with

gravity applied for the quarter model. Also, the warpage prediction from the half model is shown in Figure 6.26. The experimentally measured warpage is shown in Figure 6.27. The experimental measurements give the warpage values for the entire substrate. The modeling results shown are for a model with 8*x*8 divisions. The results from the 4*x*4 model were similar, however the model with 8*x*8 divisions seemed to be more stable in obtaining convergence.

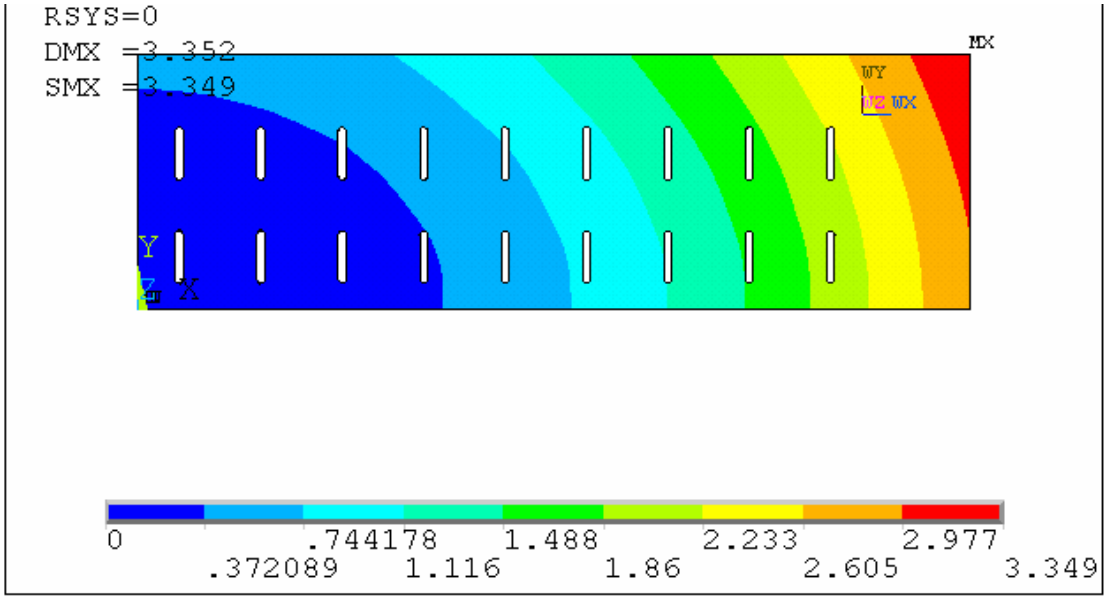

Figure 6.24: Warpage prediction before application of the gravity load

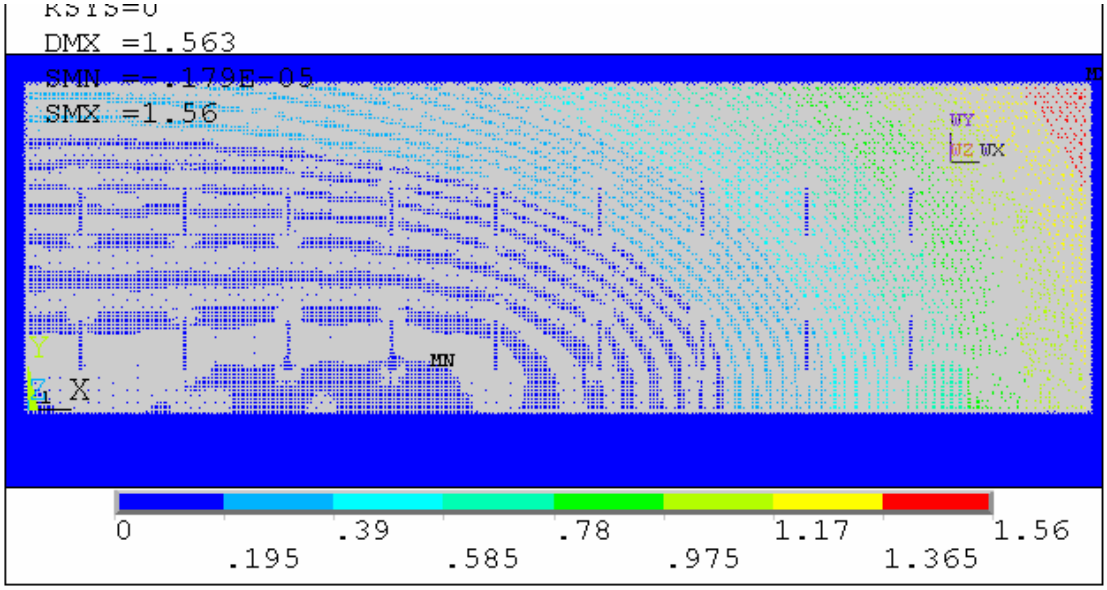

Figure 6.25: Warpage prediction after application of the gravity load

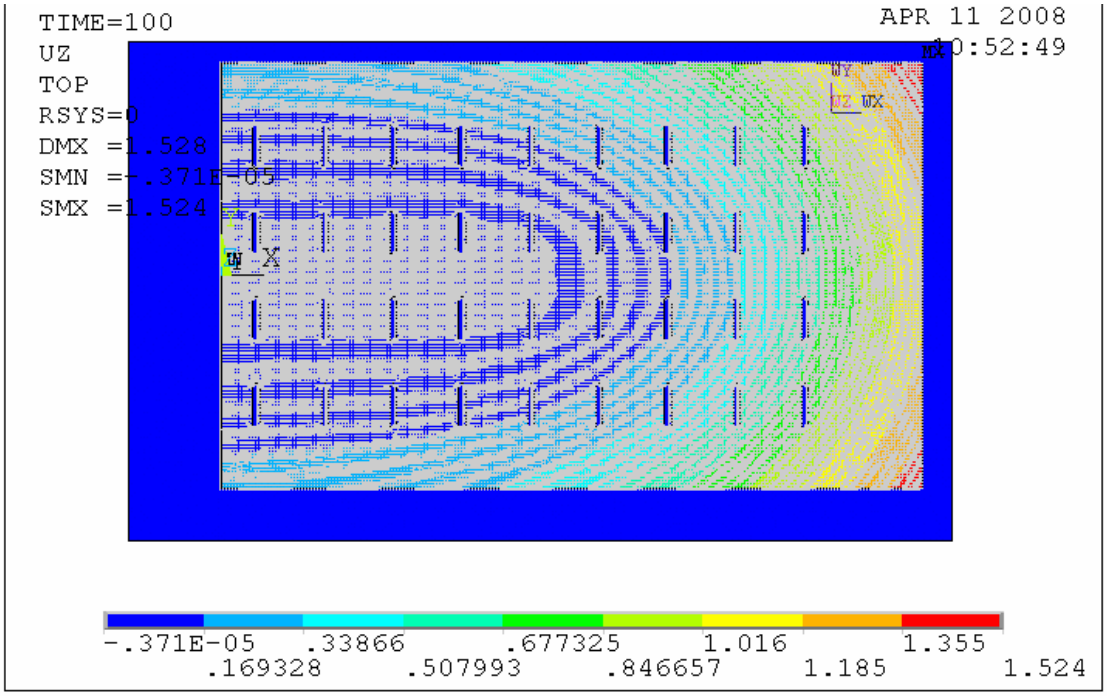

Figure 6.26: Warpage prediction from half model

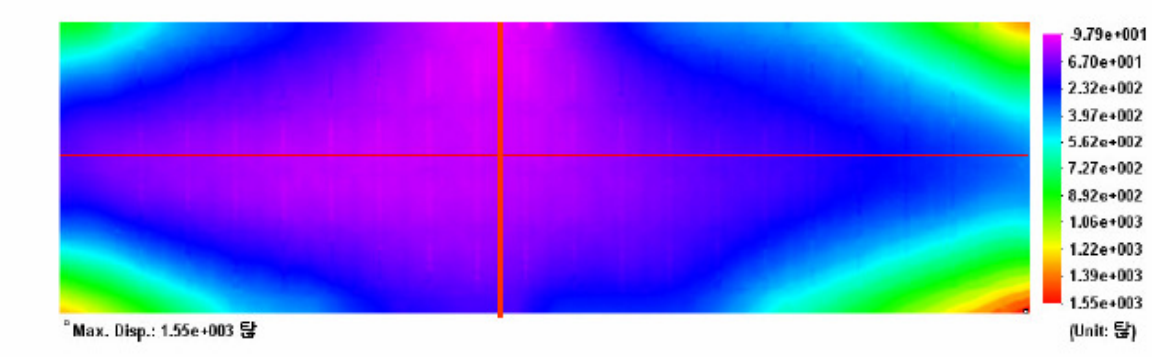

Figure 6.27: Experimental warpage measurement for previously described substrate

As shown in the figures, the warpage prediction from both the half model and the quarter model is very similar to the experimental warpage. This indicates that modeling substrates with the developed methodology leads to highly accurate results. Also, a large difference is seen between the substrate modeled with gravity applied and without gravity applied, showing the importance of modeling gravitational effects.

CHAPTER 7

PROCESSING RELATED EFFECTS

Warpage can be highly sensitive to processing related effects [Polsky, 1998]. A reel to reel process for manufacturing a particular substrate was believed to be responsible for causing a large amount of warpage in the substrate. The process in question was used to manufacture a one metal layered substrate with the stack-up shown in Figure 7.1 and the geometry shown in Figure 7.2. As seen in Figure 7.2, the substrate has quarter symmetry, so quarter symmetric boundary conditions were applied to it. The red square represents the modeled area. The material properties are the same as those given in Tables 6.1 – 6.3. The process step believed to cause most of the warpage was the application and cure of the solder resist material.

Layer	Dimension (mm)
Solder resist top	0.04
FR-4	0.15
Copper	0.018
Solder resist bottom	0.03

Figure 7.1: Material stack-up for substrate made with reel to reel process

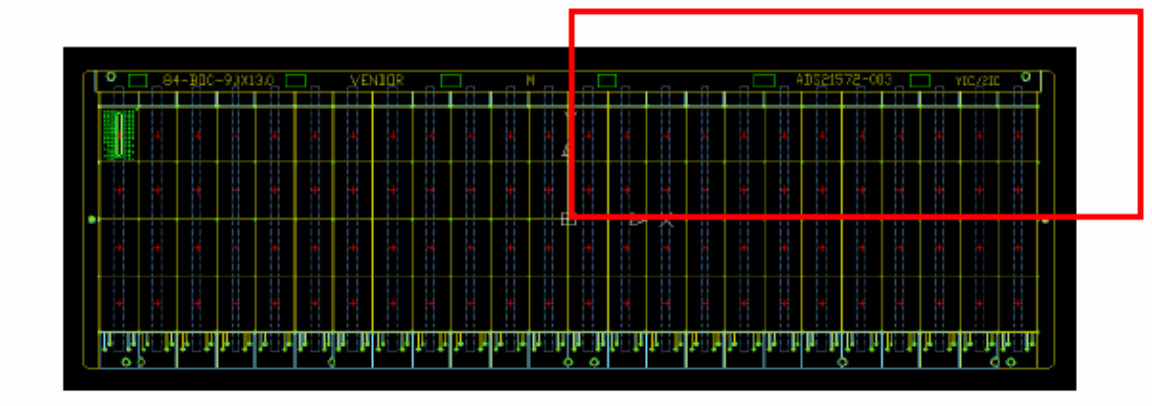

Figure 7.2: Geometry of substrate modeled

This process step starts with electroplated FR-4 on a reel. The FR-4 is then fed onto another reel. As the FR4 is fed onto the second reel, the uncured solder resist material is applied. After solder resist has been applied to all of the FR-4, the substrate will be entirely on the second reel. Spacers are placed between each revolution of the substrate around the reel to prevent contact between parts of the substrate. The reel is then placed in an oven and the dielectric is cured at 150°C. After the cure bake, the substrates are significantly warped. It is believed that this warpage is due both to thermomechanical mismatches between the constituent materials in the substrate and to cure of the solder resist taking place while the substrate is bent. It was desired to be able to capture the warpage induced from this process step using FE models.

The modeling of this process was first attempted using 3D elements with element birth and death. The substrate structure was modeled with 3D elements, and the elements for the solder resist were "killed". The structure was then bent to have a radius of curvature of the substrate when it is on the reel. The solder resist layers were then "re-born" and the substrate was cooled from the cure temperature of 150°C to room temperature. This procedure is shown in Figure 7.3.

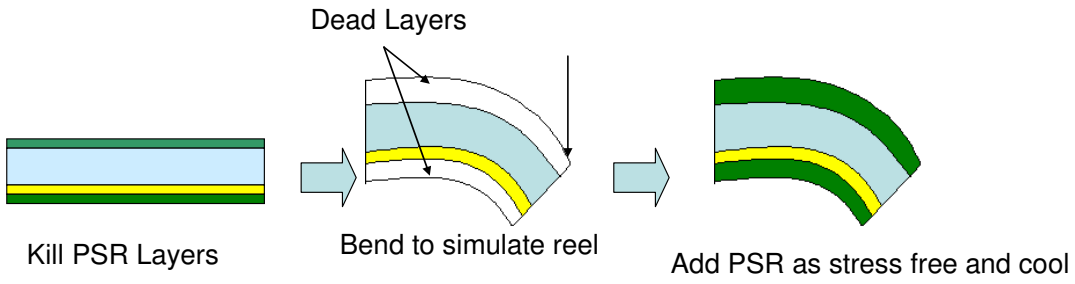

Figure 7.3: Methodology for using 3D elements

However, the holes in the substrate geometry combined with the thinness of the individual substrate layers made it difficult to mesh the model with elements with an acceptable aspect ratio without exceeding the node limit in the ANSYS student version. Therefore, an equivalent methodology using shell elements was developed.

Element birth and death can not be used with individual layers of shell elements, so the same approach used with 3D elements could not be employed. A new methodology was developed to overcome this obstacle. The first step of this methodology is to create a shell element model of the substrate with a "ghost" representation of the solder resist layers. The elastic modulus of these layers is set to 10^{-9} MPa, so they have no effect on the stresses developed in the other layers, effectively killing these layers. The structure is then bent to have the radius of curvature that the substrate on the reel has. The stress state for this structure is then saved. This yields the stress state for the substrate when it is held in a bent position but the solder resist has not yet cured.

A new model is then created with the correct material properties applied to all layers. All of the elements in this model are then "killed" and the model is bent to have the radius of curvature of the substrate on the reel. Since all the elements were killed for this step this model has zero stress. Now the stress state from the previous model is

applied to the current model, yielding a model with the stresses from bending the core and copper layers and stress free solder resist layers, which is the same state the substrate would actually be in. Now the substrate is taken from the solder resist cure temperature of 150° C to room temperature. This methodology is pictured in Figure 7.4. This simulates bending the core and copper layers with the solder resist having no modulus, then curing the solder resist so that it develops its modulus then lowering the temperature.

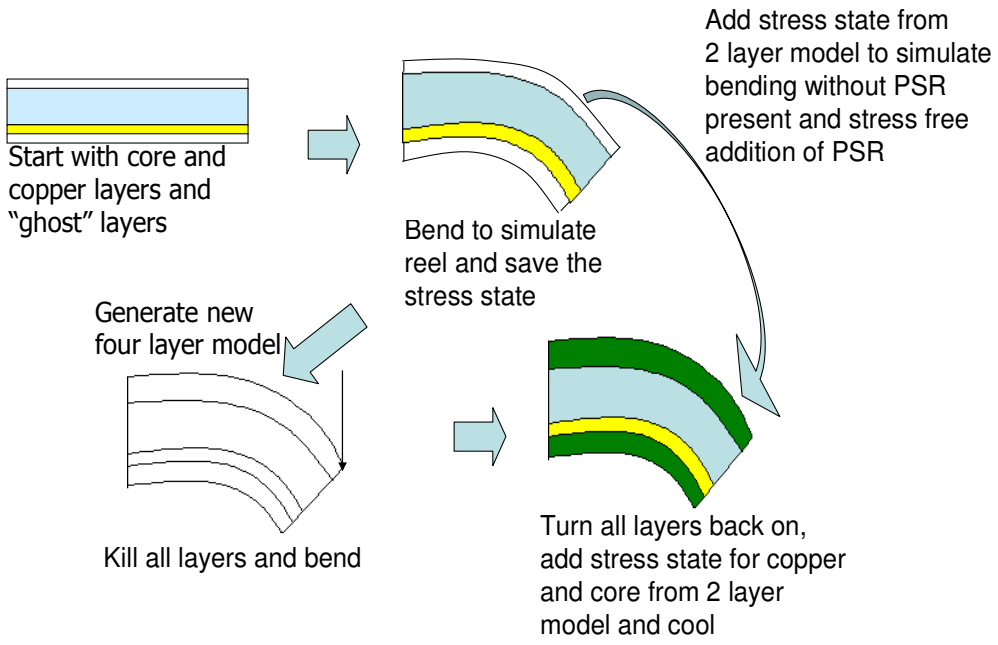

Figure 7.4:Methodology using shell elements

This methodology has one extra step than required in using the 3D methodology, however, since it uses shell elements instead of 3D elements, the processing time required is much lower. Also, this methodology allows the modeling of very thin layers in birth and death analyses, which is difficult with 3D elements.

Since this methodology is not a proven technique, it was desired to have some validation of its effectiveness and accuracy. This was done by comparing warpage predictions from using birth and death with 3D elements to using the developed

methodology for a simple substrate geometry. The substrate had a simple square geometry and was 10 mm long by 6 mm high had an isotropic trace pattern. Since the substrate was symmetric, quarter models were made for both the 3D and shell element models. The upper right hand side of the substrate was modeled in both models. The same boundary conditions which were applied to previous quarter models were applied to the current models. The modeling results for the 3D model are shown in Figure 7.5 the results for the shell element model are shown in Figure 7.6.

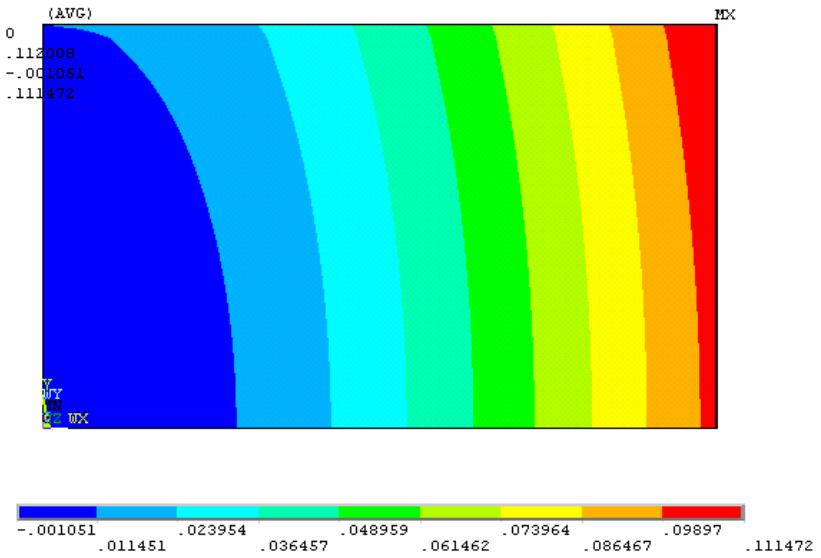

Figure 7.5: Warpage prediction from using 3D methodology to simulate reel to reel processing

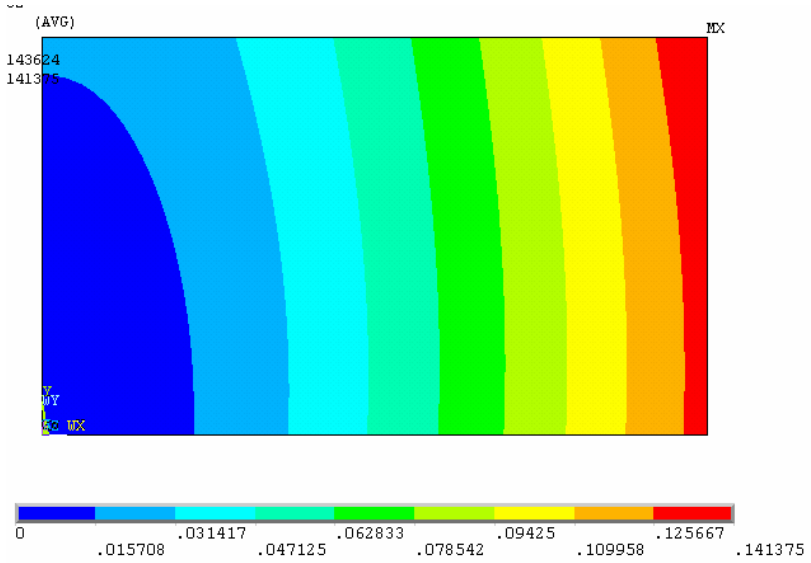

Figure 7.6: Warpage prediction from using shell elements to simulate the reel to reel process

Inspection of the two figures shows that the results predicted by each model are similar, indicating that the shell element methodology is a viable solution to overcoming the problems with the 3D methodology.

This methodology was used to model the substrate shown in Figure 7.2. The warpage prediction from this model is shown in Figure 7.7. The warpage prediction from this substrate was compared to experimental data obtained by measuring the warpage along the edge of the substrate as measured vertically from a flat plate. The warpage measurements are plotted against predicted values in Figure 7.8

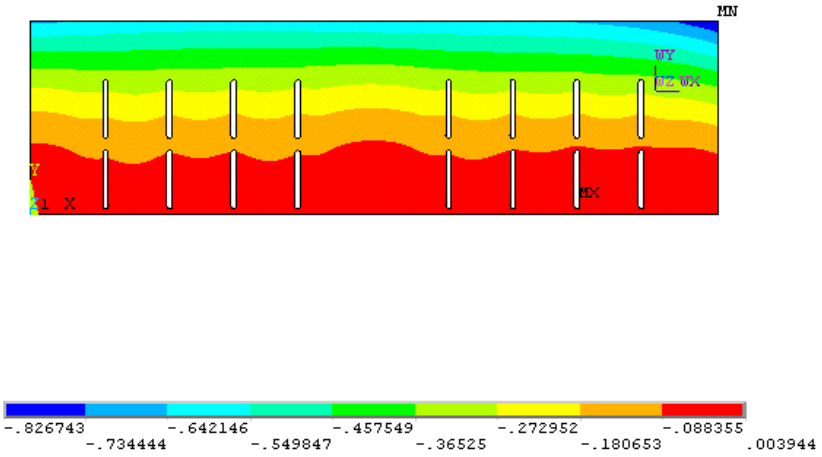

Figure 7.7: Warpage prediction for reel to reel substrate

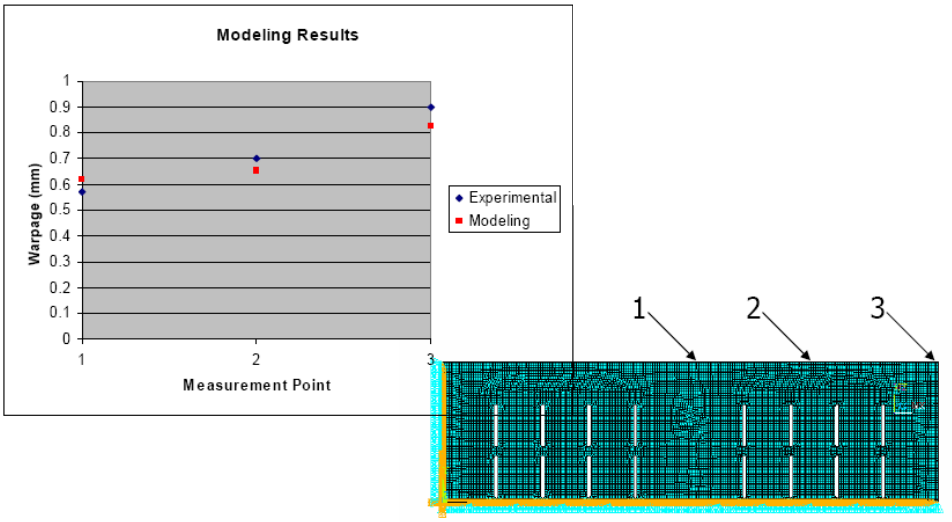

Figure 7.8: Comparison of experimental and modeling results

As seen in Figure 7.8, the predicted and experimental results are similar. Note that even though Figure 7.7 shows negative warpage, the numbers in Figure 7.8 are correct, as the measurements were done with the ball attach side up and the model was done with the chip attach side up. Note that the direction of the copper traces was taken into account for this modeling effort, but it was done by manual estimation and not by the automated technique developed in the preceding Chapters.

CHAPTER 8

CONCLUSIONS AND CONTRIBUTIONS

8.1 Conclusions

Warpage from the thermomechanical mismatches of materials used in electronic packages is a large problem in the microelectronics industry. Modeling of package substrates can be difficult, as their geometries are often complicated. Methods to model warpage with FEM often include strategies to reduce the complexity of copper trace patterns in the models and calculate the effective material properties for substrate layers which have a mix of copper and dielectric material. In this work, the current methods used to calculate effective material properties for layers of mixed copper and dielectric were reviewed and compared to models which modeled the copper trace pattern exactly. Since these strategies were found not to yield models which predict warpage with sufficient accuracy, a new methodology was developed which includes information about the orientation of copper traces when calculating effective material properties for layers of mixed copper and dielectric.

The models made using this methodology were compared both to models which represented the copper trace pattern exactly and to experimental data. Good agreement was found between models which used the developed methodology, exact substrate models, and experimental data. This showed that the developed methodology gives good results for warpage predictions. In comparisons between model types, it was found that the maximum warpage calculated by the developed methodology was on average within 16% of the maximum warpage predicted from the exact model, while the maximum warpage calculated using isotropic effective properties was on average 65% away from

the exact model. Also, predictions of the warpage contours were more accurate with the developed effective property model.

The effect of modeling gravity on the warpage of a flexible substrate was also demonstrated. Before the effect of gravity was included in the modeling simulation, the predicted warpage was nearly double the actual substrate warpage. With the inclusion of gravity loading in the simulation, the predicted warpage value became nearly the same as that given by the experimental measurements. This showed both the importance of modeling gravity when comparing warpage values to experimental results and the high accuracy obtainable from modeling mixed copper and dielectric layers with the developed methodology.

It was found that the developed methodology works best when there are a large number of traces running in a coherent direction, as this allowed the calculation of material properties which were very similar to the actual properties of the substrate layers. It proved to be more difficult to calculate material properties for trace patterns with a large number of perpendicular lines or circular patterns, and in some cases isotropic properties were used for those areas. As demonstrated, the developed methodology works well with a small number of layers. The effect of having a large number of copper layers was not tested. It was also found that increasing the number of divisions used to model a particular layer in the developed methodology does not necessarily lead to higher accuracy. Rather, there appears to be a maximum number of divisions which is needed to achieve the highest possible accuracy, and after that additional subdivisions are unnecessary.

The processing related warpage of a reel to reel process was also studied. Models of the substrate using 3D elements could not be constructed due to node restrictions in the ANSYS student version. Therefore, a methodology using shell elements was developed. This methodology yielded results similar to a methodology using 3D elements but had a greatly reduced processing time. This methodology worked well for substrates which could not be modeled with 3D elements, and also would be useful on computers which lack the processing power to model a complex substrate with 3D elements.

8.2 Summary of Contributions

- The effectiveness of modeling mixed copper and dielectric layers with volume average isotropic property models was studied and shown to lack accuracy for trace patterns with traces running in well defined directions.
- A methodology was developed which took into account the orientation of copper traces when calculating effective material properties for use in modeling
- Models made with this methodology were validated with measurements on experimental substrates using shadow Moiré
- A methodology using shell elements to model a reel to reel manufacturing process was developed. Such a model includes both volume-averaged material properties as well as direction-dependent material properties for the Cu-dielectric layer.

CHAPTER 9

FUTURE WORK

In general, substrate core materials and solder resist materials are viscoelastic, especially in the range of their T_g. However, elastic properties were used for these materials in this analysis due to lack of data to characterize them. In the future, viscoelastic data should be obtained and applied to these materials.

Also, in modeling the effective properties of the copper trace pattern, features such as vias and through holes were ignored. In the future, some method of accounting for these features should be developed.

Now that a method exists for calculating the warpage based on the direction and volume of copper in various layers, a method of optimizing the copper pattern to minimize warpage should be developed.

The warpage calculation for the reel to reel process was not verified with a full field warpage measurement. For this methodology to be accepted, the full field warpage of an actual substrate should be predicted by a model and then verified experimentally.

APPENDIX A

The ANSYS APDL code which was written for the purposes of this thesis is given here. The APDL code is used in ANSYS to build and run a finite element model of a substrate using the outputs from the MATLAB program as inputs. The second set of APDL code is used to capture reel to reel processing related effects on a small area.

A.1 APDL CODE FOR EFFECTIVE ORTHOTROPIC MODELING

```
! Make Areas
/quit
/cle
/prep7
length_x = 230
length_y = 70
x_pack = 11.27
y_pack = 14.27
x_wind = 1.1
y_wind = 7.262
y_dum1 = 6.46
x_dum2 = 13.57
x_dum1 = length_x-x_dum2
x_mid = 0
!Changed xmid to 0

x_div = 8
y_div = 8

k,,0,0,0

kp1 = _return

k,,0,length_y/2-y_dum1
kp2 = _return

k,,0,length_y/2,0
kp3 = _return

k,,length_x/2-x_dum2,0,0
kp4 = _return

k,,length_x/2,0,0
```

```
kp5 = _return

k,,length_x/2-x_dum2,length_y/2-y_dum1,0
kp6 = _return

k,,length_x/2-x_dum2,length_y/2,0
kp7 = _return

k,,length_x/2,length_y/2,0
kp8 = _return

k,,length_x/2,length_y/2-y_dum1
kp9 = _return

a,kp1,kp4,kp6,kp2

i=0
j=0
*do,b,1,1,1
*do,b,1,4,1

cyl4,i*(x_pack)+x_pack/2+x_mid,j*(y_pack)+y_pack/2-y_wind/2+x_wind/2,x_wind/2
cyl4,i*(x_pack)+x_pack/2+x_mid,j*(y_pack)+y_pack/2+y_wind/2-x_wind/2,x_wind/2
blc5,i*(x_pack)+x_pack/2+x_mid,j*(y_pack)+y_pack/2,x_wind,y_wind-x_wind
aadd,2,3,4
asba,1,5,keep,delete

i=i+1

cyl4,i*(x_pack)+x_pack/2+x_mid,j*(y_pack)+y_pack/2-y_wind/2+x_wind/2,x_wind/2
cyl4,i*(x_pack)+x_pack/2+x_mid,j*(y_pack)+y_pack/2+y_wind/2-x_wind/2,x_wind/2
blc5,i*(x_pack)+x_pack/2+x_mid,j*(y_pack)+y_pack/2,x_wind,y_wind-x_wind
aadd,1,3,4
asba,2,5,keep,delete

i=i+1

*enddo
cyl4,i*(x_pack)+x_pack/2+x_mid,j*(y_pack)+y_pack/2-y_wind/2+x_wind/2,x_wind/2
cyl4,i*(x_pack)+x_pack/2+x_mid,j*(y_pack)+y_pack/2+y_wind/2-x_wind/2,x_wind/2
blc5,i*(x_pack)+x_pack/2+x_mid,j*(y_pack)+y_pack/2,x_wind,y_wind-x_wind
aadd,2,3,4
asba,1,5,keep,delete
j=j+1
i=0
*enddo
```

```
i=0
j=1
*do,b,1,1,1
*do,b,1,4,1

cyl4,i*(x_pack)+x_pack/2+x_mid,j*(y_pack)+y_pack/2-y_wind/2+x_wind/2,x_wind/2
cyl4,i*(x_pack)+x_pack/2+x_mid,j*(y_pack)+y_pack/2+y_wind/2-x_wind/2,x_wind/2
blc5,i*(x_pack)+x_pack/2+x_mid,j*(y_pack)+y_pack/2,x_wind,y_wind-x_wind
aadd,1,3,4
asba,2,5,keep,delete

i=i+1

cyl4,i*(x_pack)+x_pack/2+x_mid,j*(y_pack)+y_pack/2-y_wind/2+x_wind/2,x_wind/2
cyl4,i*(x_pack)+x_pack/2+x_mid,j*(y_pack)+y_pack/2+y_wind/2-x_wind/2,x_wind/2
blc5,i*(x_pack)+x_pack/2+x_mid,j*(y_pack)+y_pack/2,x_wind,y_wind-x_wind
aadd,2,3,4
asba,1,5,keep,delete

i=i+1

*enddo
cyl4,i*(x_pack)+x_pack/2+x_mid,j*(y_pack)+y_pack/2-y_wind/2+x_wind/2,x_wind/2
cyl4,i*(x_pack)+x_pack/2+x_mid,j*(y_pack)+y_pack/2+y_wind/2-x_wind/2,x_wind/2
blc5,i*(x_pack)+x_pack/2+x_mid,j*(y_pack)+y_pack/2,x_wind,y_wind-x_wind
aadd,1,3,4
asba,2,5,keep,delete
j=j+1
i=0
*enddo

a,kp2,kp6,kp7,kp3
a,kp4,kp5,kp8,kp7

asel,s,loc,y,(length_y/2-y_dum1)/2

*do,b,1,9*x_div-1
wpoffs,x_pack/x_div
wprota,,,90
asbw,all
wprota,,,-90
*enddo

a=0
*do,b,1,y_div*2-1
```

```
asel,s,loc,x,0,length_x/2-x_dum2
wpoffs,,(length_y/2-y_dum1)/(y_div*2)
wprota,,90
asbw,all
wprota,,-90
a=a+1
*enddo
asel, all
aglue, all

!arsym,y,all,,,
!asel,all
!arsym,x,all
!asel,all
!aglue,all
!Define sections and mesh areas
/prep7
et,,shell181
keyopt,1,8,2

!secoffset,bot
local,11,,,,,
esys,11

asel,all
aclear,all
aatt,,,,,1

!Can change number of divisions in section numbering alone
!These numbers must be lower than or equal to those in area definition
!x_div = 8
!y_div = 8

mshape,0,2d
esize,.5
a=0
d=0
c=0
h=0
*do,k,1,2
*do,e,1,y_div
*do,f,1,x_div
*do,b,1,9
asel,s,loc,y,y_pack/(y_div*2)+d*y_pack/(y_div)+h*y_pack-
(y_pack/(y_div*2)),y_pack/(y_div*2)+d*y_pack/(y_div)+h*y_pack+(y_pack/(y_div*2))
```

```
asel,r,loc,x,x_mid+x_pack/(x_div*2)+c*x_pack/(x_div)+a*x_pack-
(x_pack/(x_div*2)),x_mid+x_pack/(x_div*2)+c*x_pack/(x_div)+a*x_pack+(x_pack/(x_
div*2))

section_num = (x_div*y_div)-(d+1)*x_div+1+c
aatt,,,,,section_num


a=a+1

amesh,all
*enddo
c=c+1
a=0
*enddo
d=d+1
c=0
a=0
*enddo
d=0
a=0
c=0
h=h+1
*enddo

!other sections
!section material properties

sectype,100,shell,,dum_2,2
secdata,.03,902,0,5
secdata,.018,908,0,5
secdata,.15,900,0,5
secdata,.018,908,0,5
secdata,.03,902,0,5

asel,a,loc,x,length_x/2-x_dum2,length_x/2

aatt,,,,,100
mshape,0,2d
esize,.5
amesh,all

sectype,101,shell,,dum_1,2
secdata,.03,902,0,5
secdata,.018,907,0,5
secdata,.15,900,0,5
```

```
secdata,.018,907,0,5
secdata,.03,902,0,5

asel,s,loc,y,length_y/2-y_dum1/2

aatt,,,,,101
mshape,0,2d
esize,.5
amesh,all

lsel,s,loc,y,0
dl,all,,uy,0
dl,all,,rotx,0
!dl,all,,uz,0

nsel,s,loc,y,0
nsel,r,loc,x,0
d,all,ux,0,,,uy,uz,rotx,roty,rotz

lsel,s,loc,x,0
dl,all,,ux,o
dl,all,,roty,0

allsel
acel,,,9.81

!Define Material Properties

!mp,ex,908,(E11_dum1+E22_dum1)/2
mp,ex,908,E11_dum1
mp,ey,908,E22_dum1
!mp,prxy,908,(v12_dum1+v21_dum1)/2
mp,prxy,908,v12_dum1
mp,prxz,908,v21,dum1
!mp,pryz,908,v21_dum1
!mp,ctex,908,(cte11_dum1+cte22_dum1)/2
mp,ctex,908,cte11_dum1
mp,ctey,908,cte22_dum1
mp,dens,908,dens_cu*dum1_sec_cu+dens_psr*(1-dum1_sec_cu)

mp,reft,908,(((E_cu*dum1_sec_cu*(reft_cu+273))+(E_psr*(1-
dum1_sec_cu)*(reft_psr+273)))/(E_cu*dum1_sec_cu+E_psr*(1-dum1_sec_cu)))-273

!dummy 2
E11_dum2 = (E_cu*dum2_sec_cu+E_psr*(1-dum2_sec_cu))
E22_dum2 = (E_cu*E_psr)/(E_cu*(1-dum2_sec_cu)+E_psr*dum2_sec_cu)
```

```
v12_dum2 = vxy_cu*dum2_sec_cu+vxy_psr*(1-dum2_sec_cu)
v21_dum2 = (E22_dum2/E11_dum2)*v12_dum2

cte11_dum2=(ctex_cu*E_cu*dum2_sec_cu+ctex_psr*E_psr*(1-
dum2_sec_cu))/(E11_dum2)
cte22_dum2=(1+vxy_cu)*ctex_cu*dum2_sec_cu+(1+vxy_psr)*ctex_psr*(1-
dum2_sec_cu)-cte11_dum2*v12_dum2

!mp,ex,907,(E11_dum2+E22_dum2)/2
mp,ex,907,E11_dum1
mp,ey,907,E22_dum2
!mp,prxy,907,(v12_dum2+v21_dum2)/2
mp,prxy,907,v12_dum1
mp,prxz,907,v21,dum2
!mp,pryz,907,v21_dum2
!mp,ctex,907,(cte11_dum2+cte22_dum2)/2
mp,ctex,907,cte11_dum1
mp,ctey,907,cte22_dum2
mp,dens,907,dens_cu*dum2_sec_cu+dens_psr*(1-dum2_sec_cu)

mp,reft,907,(((E_cu*dum2_sec_cu*(reft_cu+273))+(E_psr*(1-
dum2_sec_cu)*(reft_psr+273)))/(E_cu*dum2_sec_cu+E_psr*(1-dum2_sec_cu)))-273

!Import Matlab Data
/input,importA,txt
/input,g12import
!/input,mat_prop_proj_new4
total = info(1,1)*info(1,2)

*do,global_position,1,total,1
mp,ex,global_position,E11(global_position)!+.1*E11(global_position)
mp,ey,global_position,E22(global_position)!+.1*E22(global_position)
mp,ez,global_position,E22(global_position)!rerun this test
mp,prxy,global_position,v12(global_position)
mp,prxz,global_position,v21(global_position)
mp,pryz,global_position,v21(global_position)
mp,ctex,global_position,cte11(global_position)
mp,ctey,global_position,cte22(global_position)
!mp,ez,global_position,E22(global_position)
mp,gxy,global_position,g12(global_position)
mp,gyz,global_position,g12(global_position)*.25
!mp,gxz,global_position,g12(global_position)*.25
mp,gxz,global_position,g12(global_position)
mp,reft,global_position,reft(global_position)
mp,dens,global_position,dens(global_position)
```

```
tb,prony,global_position,1,3,shear
tbdata,1,(1-(p1*E_psr)/E(global_position)),5,.5,50
*enddo

!BA up
*do,position,1,info(1,1),1
sectype,position,shell,,main1,0
secdata,.03,3,0,5 !BA
secdata,.018,position+info(1,1),angle(position+info(1,1)),5
secdata,.15,900,0,5
secdata,.018,position,angle(position),5
secdata,.03,3,0,5 !CA
*enddo
!ImportA file
/prep7
*dim, info, array,1,2
*vread, info(1,1), info,txt,,JIK,2,1
(2F12.8)

*dim, percent, array,info(1,1)*info(1,2)
*vread, percent(1,1), percent,txt,,IJK,info(1,1)*info(1,2)
(F12.8)

*dim, angle, array,info(1,1)*info(1,2)
*vread, angle(1,1), angle,txt,,IJK,info(1,1)*info(1,2)
(F12.8)

*dim, E11, array,info(1,1)*info(1,2)
*vread, E11(1,1), E11,txt,,IJK,info(1,1)*info(1,2)
(F12.8)

*dim, E22, array,info(1,1)*info(1,2)
*vread, E22(1,1), E22,txt,,IJK,info(1,1)*info(1,2)
(F12.8)

*dim, v12, array,info(1,1)*info(1,2)
*vread, v12(1,1), v12,txt,,IJK,info(1,1)*info(1,2)
(F12.8)

*dim, v21, array,info(1,1)*info(1,2)
*vread, v21(1,1), v21,txt,,IJK,info(1,1)*info(1,2)
(F12.8)

*dim, cte11, array,info(1,1)*info(1,2)
*vread, cte11(1,1), cte11,txt,,IJK,info(1,1)*info(1,2)
(F12.8)
```

```
*dim, cte22, array,info(1,1)*info(1,2)
*vread, cte22(1,1),cte22,txt,,IJK,info(1,1)*info(1,2)
(F12.8)

*dim, reft, array,info(1,1)*info(1,2)
*vread, reft(1,1),reft,txt,,IJK,info(1,1)*info(1,2)
(F12.8)

*dim, dens, array,info(1,1)*info(1,2)
*vread, dens(1,1),dens,txt,,IJK,info(1,1)*info(1,2)
(F12.8)

!*DIM,EXAMPLE,,2,3
!*VREAD,EXAMPLE(1,1),dataval,,,JIK,3,2
!(3F6.1)

!g12import file
*dim, G12, array,info(1,1)*info(1,2)
*vread, G12(1,1),G12,txt,,IJK,info(1,1)*info(1,2)
(F12.8)

!Place plate below substrate for gravity model
!wpoffs,,,-.1
blc4,-.25-length_x/2,-.25-length_y,length_x/2+20,length_y+12

blc4,-.25-length_x/2,-.25-length_y/2,length_x/2+20,length_y/2+12
!wpoffs,x_pack/4

asel,s,loc,y,-5,0
asel,r,loc,x,length_x/4-10,length_x/4+10
blc4,-length_x-.25,-length_y-.25,length_x+x_dum2,length_y+y_dum1+1

asel,s,area,,3
nsla,s,all

!nsel,s,loc,y,0
!nsel,r,loc,x,0
d,all,ux,0,,,uy,uz,rotx,roty,rotz

!Cool Substrate
allsel,all
/solu
tref,175
KBC,0
NSUBST,35,77,1
```

```
AUTOTS,ON
NROPT,FULL,,ON                !USE FULL NEWTON RAPHSON WITH ADAPTIVE
DESCENT
SSTIF,ON                      !INCLUDE STRESS STIFFENING
NLGEOM,ON                     !INCLUDE LARGE DEFORMATION EFECTS
EQSLV,SPARSE
TOFFST,273,                   !SET THE TEMP OFFSET FROM ABSOLUTE ZERO TO
273
NEQIT,200                     !SET 100 AS MAX NUMBER OF EQUIL ITERATIONS
time,100
allsel,all
bf,all,temp,25
outres,all,last
solve
```

A.2 APDL CODE FOR REEL TO REEL PROCESS MODEL

```
/quit
/cle
/prep7

length_x = 220
length_y = 62
x_pack = 10.27
y_pack = 11.27
x_wind = .9
y_wind = 9.375
y_dum1 = 8.46
x_dum2 = 7.3
x_dum1 = length_x-x_dum2
x_mid = 0

k,,0,0,0
k,,5,0,0
k,,5,3,0
k,,0,3,0

l,1,2
l,2,3
l,3,4
l,4,1

al,1,2,3,4
et,,shell181
```

```
keyopt,1,8,2

sectype,1,shell,,main1,0
secdata,.04,10,0,5 !BA
secdata,.018,4,0,5
secdata,.15,1,0,5
secdata,.03,10,0,5 !CA

local,11,,,,,
esys,11

mshape,0,2d
esize,.1
asel,all
aatt,,,,,1
amesh,all

dl,1,,rotx,0
dl,1,,uy,0
dl,4,,uz,0        !hold

dl,4,,roty,0
dl,4,,ux,0

lsel,s,loc,x,0
lsel,r,loc,y,0
dl,all,,uz,0
d,1,all,all
!dl,all,,rotz,0

/input,area_exp_new
/input,sections_and_loads_exp_new
/input,mat_prop_proj_new2

/solu
tref,55
nlgeom,on
nropt,full
neqit,200
antype,0
eqslv,sparse
time,100
allsel,all
!bf,all,temp,150
lsel,s,loc,x,5
dl,all,,uz,.523
```

```
outres,all,last
iswrite,on
allsel,all
solve
save,firstA2,solu

/quit
/cle
/prep7

length_x = 220
length_y = 62
x_pack = 10.27
y_pack = 11.27
x_wind = .9
y_wind = 9.375
y_dum1 = 8.46
x_dum2 = 7.3
x_dum1 = length_x-x_dum2
x_mid = 0


k,,0,0,0
k,,5,0,0
k,,5,3,0
k,,0,3,0

l,1,2
l,2,3
l,3,4
l,4,1

al,1,2,3,4

et,,shell181
keyopt,1,8,2

sectype,1,shell,,main1,0
secdata,.04,3,0,5 !BA
secdata,.018,4,0,5
secdata,.15,1,0,5
!secdata,.018,4,0,5
secdata,.03,3,0,5 !CA

local,11,,,,,
esys,11
```

```
mshape,0,2d
esize,.1
asel,all
aatt,,,,,1
amesh,all

dl,1,,rotx,0
dl,1,,uy,0
dl,4,,uz,0

dl,4,,roty,0
dl,4,,ux,0

lsel,s,loc,x,0
lsel,r,loc,y,0
dl,all,,uz,0
d,1,all,all
!dl,all,,rotz,0

/input,mat_prop_proj_new2

/solu
tref,150 !CHANGE TO 150
nlgeom,on
nropt,full
neqit,200
antype,0
eqslv,sparse
time,100
allsel,all
!bf,all,temp,150
lsel,s,loc,x,5
dl,all,,uz,.523
outres,all,last
isfile,read,3dthirdB,,,1,1,4,3
isfile,list,all
iswrite,off
esel,all
ekill,all
allsel,all
solve
save,secondA3,solu

/solu
tref,25
```

```
nlgeom,on
nropt,full
neqit,200
antype,0
eqslv,sparse
time,100
allsel,all
bf,all,temp,25
lsel,s,loc,x,5
dl,all,,uz,.523
lsel,s,loc,x,5
nsll,s,1
ddele,all,all
dldele,all,all
lsel,s,loc,x,0
nsll,s,1
dldele,all,uz
ddele,all,uz
d,1,all,all
outres,all,last
!isfile,read,3dthirdB,,,1,1,4,3
!isfile,list,all
iswrite,on
esel,all
ealive,all
allsel,all
solve
save,testB,solu

/solu
tref,150
nlgeom,on
nropt,full
neqit,200
antype,0
eqslv,sparse
time,100
allsel,all
bf,all,temp,25
!lsel,s,loc,x,5
!dl,all,,uz,.523
outres,all,last
esel,all
ealive,all
!isfile,read,3dA,,,1,1,4,3
!isfile,list,all
```

```
!iswrite,on
!lsel,s,loc,x,5
!nsll,s,1
!dldele,all,all
!ddele,all,all
allsel,all
solve
save,thirdA3,solu

/solu
tref,150
nlgeom,on
nropt,full
neqit,200
antype,0
eqslv,sparse
time,100
allsel,all
bf,all,temp,25
!lsel,s,loc,x,41.3
!dl,all,,uz,1.75
outres,all,last
esel,all
ealive,all
lsel,s,loc,x,5
nsll,s,1
dldele,all,all
ddele,all,all
lsel,s,loc,x,0
nsll,s,1
dldele,all,uz
ddele,all,uz
d,1,all,all
!isfile,read,lukemain,,,1,1,4
!iswrite,on
allsel,all
solve
save,fourthA3,solu



/solu
esel,all
ealive,all
tref,55
nlgeom,on
```

```
nropt,full
neqit,200
antype,0
eqslv,sparse
time,100
allsel,all
bf,all,temp,25
lsel,s,loc,x,41.3
nsll,s,1
dldele,all,all
ddele,all,all
dl,1,,uy,0
outres,all,last
iswrite,on
allsel,all
solve
save,fifth,solu
```

REFERENCES

1. Banerji et. al. 2002 "The Role of Stiff Base Substrates in Warpage Reduction for Future High-Density-Wiring Requirements," *Proc of the 8th International Symposium on Advanced Packaging Materials*, pp 221-225

2. Corbin, J.S. 1993 "Finite element analysis for Solder Ball Connect (SBC) structural design optimization" *IBM J. Research and Development*, VOL. 31 (5) pp. 585-596

3. Dang et. al. 2000, "Process Induced Warpage in Multitiled Alumina Substrates for Large Area MCM-D Processing," *IEEE Transactions on Advanced Packaging*, 23 3), pp. 436-446

4. Daniel et. al. 1990, "Thermomechanical Behavior of Multilayer Structures in Microelectronics," *ASME J. of Electronic Packag*ing, 112 (1), pp. 11-15

5. Dharba and Dasgupta, 2001, "A Nested Finite Element Methodology (NEFM) for Stress Analysis of Electronic Products – Part I: Theory and Formulaton," *ASME J. of Electronic Packaging*, 123 (2) pp. 141-146

6. Ding, 2003, "Prediction and Validation of Thermomechanical Reliability in Electronic Packaging," Ph.D. Thesis, School of Mechanical Engineering, Georgia Institute of Technology, Atlanta

7. Ding, 2003 "Warpage Measurement Comparison Using Shadow Moiré and Projection Moiré Methods," *IEEE Transactions on Components and Packaging Technologies*, Vol 25 (4) Dec. 2002 pp. 714-721

8. Ding, 2004 "Warpage Analysis of Underfilled Wafers," *Journal of Electronic Packaging*, June 2004 Vol. 126 pp. 265-270

9. Douglass et. al., 1980, "Stresses Due to Environmental Conditioning of Cross-Ply Graphite/ Epoxy Laminates," Proceedings of ICCM-3, Vol 1, pp. 529-542.

10. Duda and Hart, "Use of the Hough Transform to Detect Lines and Curves in Pictures," *Comm. ACM* Jan. 1972, pp. 11-15

11. Dunne 2000, "An Integrated Process Modeling Methodology and Module for Sequential Multilayered High-Density Substrate Fabrication for Microelectronic Packages," Ph.D. Thesis, School of Mechanical Engineering, The Georgia Institute of Technology, Atlanta, GA

12. Farley et. al. 1978, "Influence of Two-Dimensional Hygrothermal Gradients on Interlaminar Stress Near Free Edges," *Advanced Composite Materials – Environmental Effects*, ASTM STP 658, 1978 pp. 143-159

13. Grenestedt and Hutapea (2003), "Influence of electric artwork on thermomechanical properties and warpage," *Journal of Applied Physics*, Vol 94 (1) July 2003, pp. 686-696

14. Harper 1983, "On the Effects of Post Cure Cool Down on Environmental Conditioning on Residual Stresses in Composite Laminates," Ph.D. Thesis

15. Herakovich, 1998, *Mechanics of Fiborous Composites*, John Wiley & Sons, Inc., New York, NY

16. Hough, P.V.C, *Machine Analysis of Bubble Chamber Pictures,* Proc. Int. Conf. High Energy Accelerators and Instrumentation, 1959

17. Hutapea and Grenestedt (2004 "Tuning of Artworks of Printed Circuit Boards to Reduce Warpage," *9th Int'l Symposium on Advanced Packaging Materials*, 2004 pp. 230-234.

18. Hutapea and Grenestedt, 2007 "Modifying Electric Artworks to Improve Dimensional Stability of Microelectronic Substrates," *Microelectronics International*, Vol. 24 (1) 2007, pp. 15-22

19. Lau, and Erasmus, June 1993 "Review of Packaging Methods to Complement IC Performance," *Electronic Packaging & Production,* pp. 51-56.

20. Lee & Tobin, 1986 "The Effect of CMOS Processing on Oxygen Precipitation, Wafer Warpage, and Flatness," *Journal of the Electrochemical Society*, 133 (10), pp. 2147-2152

21. Lee 1998, "Finite element analysis for solder ball failures in chip scale package," *Microelectronics and Reliability,* Vol. 38 (12), December 1998, Pages 1941-1947

22. Mallick, *Fiber Reinforced Composites*, Marcell Dekker, Inc., New York, NY, 1988.

23. Polsky, Y., 1998, "Improved Prediction Modeling with Validation for Thermally-Induced PWB Warpage," Ph. D. Thesis, School of Mechanical Engineering, Georgia Institute of Technology, Atlanta

24. Polsky, Y et. al., 2000, "A Comparison of PWB Warpage Due to Simulated Infrared and Wave Soldering Processes," IEEE Transactions on Electronic Package Manufacturing, 23 (3), pp. 191-199.

25. Polsky, 2000, "Thermoelastic Modeling of a PWB With Simulated Circuit Traces Subjected to Infrared Reflow Soldering With Experimental Validation," *Journal of Electronic Packaging*, December 1999, Vol 121 (4) pp. 263-270

26. Ranjan et. al. 1998, "Die Cracking in Flip Chip Assemblies," *Electronic Components and Technology Conference, 1998. 48th IEEE*, May 1998, pp. 729-733.

27. Reddy et. al. 1989, "On Refined Computational Models of Composite Laminates," *International Journal for Numerical Methods in Engineering*, 27 (2), pp. 361-382.

28. Reitz, S. et. al., 2002, "System Level Modeling of Microsystems Using Order Reduction Methods," *Proceedings of SPIE*, 4755, pp. 365-373

29. Rymaszewksi, Tummala, and Watari, 1999, "Microelectronics Packaging - An Overview," in *Microelectronics Packaging Handbook: Part III*, Eds. Tummala, Rymaszewski and Klopfenstein, Chapter 15, Kluwer Academic Publishers, Norwell, MA

30. Tummala, R., Rymaszewski E. J., Klopfenstien, A. G., (eds) 1997, *Microelectronics Packaging Handbook*, 2nd Edition, Chapman and Hall, New York

31. Tumala, R., *Fundamentals of Microsystems Packaging*, 2001, McGraw-Hill, New York, NY

32. Ume and Martin, 1997 "Finite Element Analysis of PWB Warpage Due to the Solder Masking Process," *IEEE Transactions on Comp. Packaging and Manufacturing Tech.,* Vol. 20 (3), September, 1997, pp. 295-306

33. Ume and Martin, 1997 "Finite Element Analysis of PWB Warpage Due to Cured Solder Mask – Sensitivity Analysis," *IEEE Transactions on Comp. Packaging and Manufacturing Tech.,* Vol. 20 (3), September, 1997, pp. 307-316

34. Variyam and Sitaraman, 2000, "Role of Out-of-Plane Coefficient of Thermal Expansion in Electronic Packaging Modeling," *ASME Journal of Electronic Packaging*, 122 (2), pp. 121-127

35. Verma et. al., 1999, "Development of Real Time/Variable Sensitivity Warpage Measurement Technique and its Application to Plastic Grid Array Package," *IEEE Transactions of Electronics Packaging Manucacturing*, 22 (1) pp. 63-70.

36. Wang et. al., 1992, "Thermoviscoelastic Analysis of Residual Stresses and Warpage in Composite Laminates," *Journal of Composite Materials*, 26 (6), pp. 889-889

37. Wang et. al. 2000, "Interfacial shear stress, peeling stress, and die cracking stressin trilayer electronic assemblies," *IEEE Transactions on Components and Packaging Technologies*, Vol 23 (2) June 2000 pp. 309 – 316.

38. White and Hahn, 1992, "Process Modeling of Composite Materials: Residual Stress Development During Cure. Part I. Model Formulation," *Journal of Composite Materials*, Vol. 26 (16) 1992, pp. 2402-2421

39. Xie and Sitaraman, 2000, "Interfacial Thermal Stress Analysis of Anisotropic Multi-Layered Electronic Packaging Structures," *Journal of Electronic Packaging*, March 2000, Volume 122, Issue 1, pp. 61-66

40. Yao and Qu, 1999, "Three-Dimensional Versus Two-Dimensional Finite Element Modeling of Flip-Chip Packages," *ASME Journal of Electronic Packaging*, 121 (3), pp. 196-201.

41. Yeh et. al., "Experimental and Analytical Investigation of Thermally Induced Warpage for Printed Wiring Boards," Electronic Components and Technology Conference, 1991. Proceedings., 41st, pp. 382-387

42. Yeh et. al., 1993, "Correlation of Analytical and Experimental Approaches to Determine Thermally Induced PWB Warpage," *IEEE Transactions of Components, Hybrids, & Manufacturing Technology*, 16 (8), pp. 986-995.

43. Zewi et. al., 1986, "Residual Stresses in Woven Glass/Epoxy Laminates," *Experimental Mechanics.* Vol. 27 (1), March, 1987, pp. 44-50

44. Zweben C., "Advances in Materials for Optoelectronic, Microelectronic, and MOEMS/MEMS Packaging," *18th IEEE SEMI-THERM Symposium,* 2002, pp. 30-34

45. Zwemer et al., 2004, "PWB Warpage Analysis and Verification using an AP210 Standards-based Engineering Framework and Shadow Moiré," *5th. Int. Conf on Thermal and Mechanical Simulation and Experiments in Micro-electronics and Micro-Systems*, 2004, pp. 121-131